OPEN ACCESS Freely available online

PLOS | ONE

N-Glycans: Phenotypic Homology and Structural Differences between Myocardial Cells and Induced Pluripotent Stem Cell-Derived Cardiomyocytes

Takuji Kawamura[1], Shigeru Miyagawa[1], Satsuki Fukushima[1], Akira Yoshida[2], Noriyuki Kashiyama[1], Ai Kawamura[1], Emiko Ito[1], Atsuhiro Saito[1], Akira Maeda[3], Hiroshi Eguchi[3], Koichi Toda[1], Jong-Kook Lee[2], Shuji Miyagawa[3], Yoshiki Sawa[1]*

1 Department of Cardiovascular Surgery, Osaka University Graduate School of Medicine, Suita, Osaka, Japan, **2** Department of Cardiovascular Regenerative Medicine, Osaka University Graduate School of Medicine, Suita, Osaka, Japan, **3** Division of Organ Transplantation, Department of Surgery, Osaka University Graduate School of Medicine, Suita, Osaka, Japan

Abstract

Cell surface glycans vary widely, depending on cell properties. We hypothesized that glycan expression on induced pluripotent stem cells (iPSCs) might change during cardiomyogenic differentiation toward the myocardial phenotype. *N*-glycans were isolated from iPSCs, iPSC-derived cardiomyocytes (iPSC-CM), and original C57BL/6 mouse myocardium (Heart). Their structures were analyzed by a mapping technique based on HPLC elution times and MALDI-TOF/MS spectra. Sixty-eight different *N*-glycans were isolated; the structures of 60 of these *N*-glycans were identified. The quantity of high-mannose type (immature) *N*-glycans on the iPSCs decreased with cardiomyogenic differentiation, but did not reach the low levels observed in the heart. We observed a similar reduction in neutral *N*-glycans and an increase in fucosylated or sialyl *N*-glycans. Some structural differences were detected between iPSC-CM and Heart. No *N*-glycolyl neuraminic acid (NeuGc) structures were detected in iPSC-CM, whereas the heart contained numerous NeuGc structures, corresponding to the expression of cytidine monophosphate-*N*-acetylneuraminic acid hydroxylase. Furthermore, several glycans containing Galα1-6 Gal, rarely identified in the other cells, were detected in the iPSC-CM. The expression of *N*-glycan on murine iPSCs changed toward the myocardial phenotype during cardiomyogenic differentiation, leaving the structural differences of NeuGc content or Galα1-6 Gal structures. Further studies will be warranted to reveal the meaning of the difference of *N*-glycans between the iPSC-CM and the myocardium.

Citation: Kawamura T, Miyagawa S, Fukushima S, Yoshida A, Kashiyama N, et al. (2014) *N*-Glycans: Phenotypic Homology and Structural Differences between Myocardial Cells and Induced Pluripotent Stem Cell-Derived Cardiomyocytes. PLoS ONE 9(10): e111064. doi:10.1371/journal.pone.0111064

Editor: Toru Hosoda, Tokai University, Japan

Received April 30, 2014; **Accepted** September 19, 2014; **Published** October 30, 2014

Data Availability: The authors confirm that all data underlying the findings are fully available without restriction. All relevant data are within the paper and its Supporting Information files.

Funding: YS received the funding to support this work from the Research Center Network for Realization of Regenerative Medicine managed by Centers for Clinical Application Research on Specific Disease/Organ and funded by Japan Science and Technology Agency. The funders had no role in study design, data collection and analysis, decision to publish, or preparation of the manuscript.

Competing Interests: The authors have declared that no competing interests exist.

* Email: sawa-p@surg1.med.osaka-u.ac.jp

Introduction

In vitro generation of cardiac myocytes by reprogramming is a promising technology in developing cell-transplant therapy for advanced cardiac failure [1] and drug discovery for a variety of cardiac diseases [2]. For both purposes, induced pluripotent stem cells (iPSCs) are most useful, since generation and cardiomyogenic differentiation of iPSCs has been standardized in human and a number of animals [3,4]. In fact, derivatives of iPSCs have been developed to the pre-clinical stage for cell transplantation therapy [5], while cardiac myocytes generated from patient-specific iPSCs have been studied to explore pathologic mechanisms and guide drug discovery [6,7]. However, cardiac myocyte preparations from iPSCs contain immature phenotypes, observed by electrophysiology, electron microscopy, and immunohistochemistry [8,9]; this may limit the safety and efficacy of cell transplantation therapy or reduce the accuracy and efficiency of drug discovery. The maturity of iPSC-derived cardiac myocytes (iPSC-CMs) has not been comprehensively or quantitatively evaluated.

Cell surface glycans have several important functions interacting with numerous proteins, including growth factors, morphogens and adhesion molecules, modulating dynamic cellular mechanisms such as cell-cell adhesion, cell activation, and malignant alterations [10–12]. In early mammalian embryos, associated with fertilization, some *N*-glycans play important roles of cell-cell adhesion [13–15]. In addition, cellular responsiveness to growth or arrest depends on total *N*-glycan number and the degree of branching of cell surface glycoproteins [16]. Furthermore, heparan sulfate, a kind of glycans, is required for embryonic stem cell (ESC) pluripotency, in particular lineage specification into mesoderm through facilitation of FGF and BMP signaling by stabilizing BMP ligand [17], leading the evidence that the expression patterns of cell surface glycans on ESCs changes during differentiation [18]. Thus, we hypothesized that cell surface glycan expression may

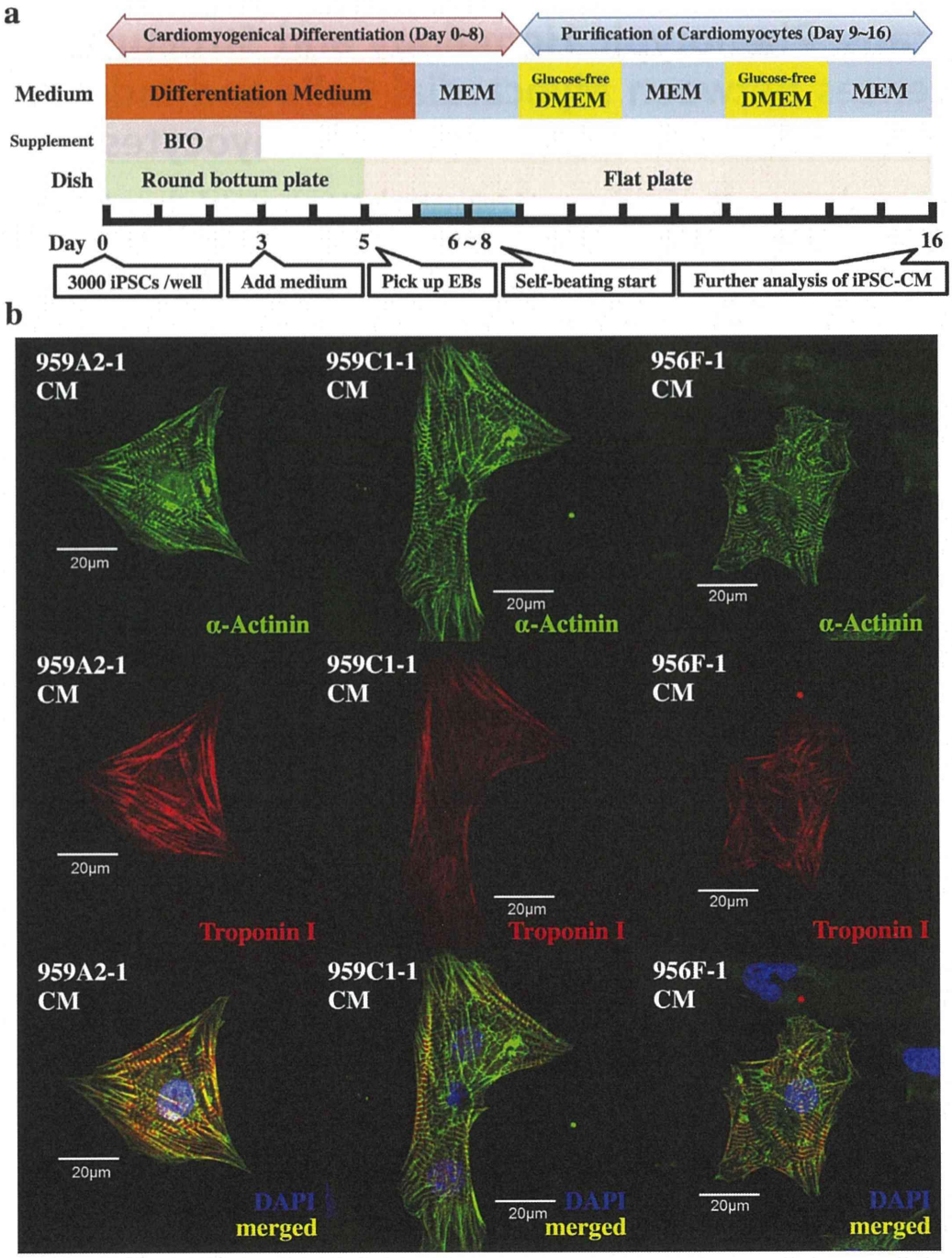

Figure 1. Cardiomyogenic differentiation of iPSCs and cardiomyocyte purification. (a) The cardiomyogenic differentiation protocol and cardiomyocyte purification process are illustrated. (b) IPSC-CMs stained with anti-α-actinin antibody (Alexa Fluor 488), anti-troponin I (Alexa Fluor 594) and DAPI, were analyzed with a confocal laser scanning microscopy. Abbreviations: EB, embryonic body; MEM, Modified Eagle's Medium; DMEM, Dulbecco's Modified Eagle's Medium; BIO, 6-bromoindirubin-3′-oxime.
doi:10.1371/journal.pone.0111064.g001

change during the course of cardiomyogenic differentiation of iPSCs *in vitro*. We analyzed *N*-glycan expression in undifferentiated iPSCs, iPSC-CMs, and adult murine myocardium by HPLC, to identify potential indicators of the maturity of differentiating cardiomyocytes from iPS cells *in vitro*.

Materials and Methods

Animal care procedures were consistent with the "Guide for the Care and Use of Laboratory Animals" (National Institutes of Health publication). Experimental protocols were approved by the

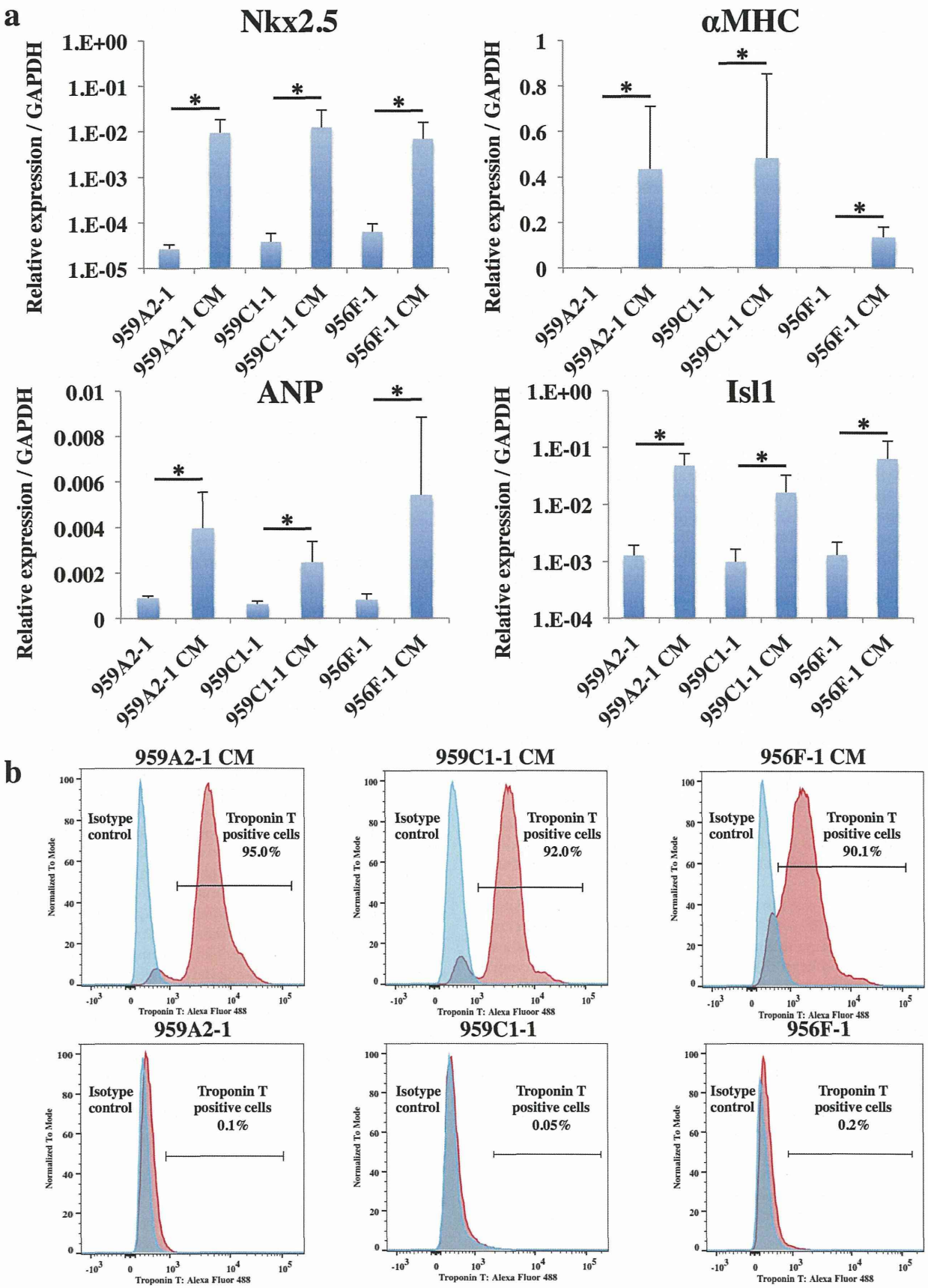
a
Nkx2.5
αMHC
ANP
Isl1
Relative expression / GAPDH
959A2-1
959A2-1 CM
959C1-1
959C1-1 CM
956F-1
956F-1 CM
b
959A2-1 CM
959C1-1 CM
956F-1 CM
959A2-1
959C1-1
956F-1
Isotype control
Troponin T positive cells 95.0%
Troponin T positive cells 92.0%
Troponin T positive cells 90.1%
Troponin T positive cells 0.1%
Troponin T positive cells 0.05%
Troponin T positive cells 0.2%
Normalized To Mode
Troponin T: Alexa Fluor 488

Figure 2. Highly purified iPSC-CMs expressing cardiomyocyte marker genes. (a) Transcript expression of Nkx2.5, αMHC, ANP and Isl1 in the iPSCs and the iPSC-CMs were analyzed by real-time PCR. Results are expressed as the mean ± standard deviation. *P<0.05. (b) IPSC-CMs and iPSCs stained with anti-troponin T antibody or the isotype control, followed by Alexa Fluor 488-conjugated anti-mouse IgG antibody, were analyzed by flow cytometry.
doi:10.1371/journal.pone.0111064.g002

Ethics Review Committee for Animal Experimentation of Osaka University Graduate School of Medicine.

Cardiomyogenic differentiation of murine iPSCs *in vitro*

We used the murine iPSC lines, 959A2-1, 959C1-1, 956F-1 (generous gifts from Dr. Okita and Professor Yamanaka of the Center for iPS Cell Research and Application, Kyoto University, Kyoto, Japan). The cell lines were generated from C57BL/6 (B6) (CLEA) mouse embryonic fibroblasts by introducing *Oct3/4, Sox2, Klf4*, and *c-Myc* without viral vectors as described [19]. The iPSCs were cultured in the absence of serum and feeder cells by using ESGRO Complete PLUS Clonal Grade Medium (Millipore).

Cardiomyogenic differentiation of the iPSCs was performed as described [20,21], with modifications, followed by purification with glucose-free medium supplemented with lactic acid [22]; iPSCs (3×10^3) were resuspended in 100-μL aliquots of differentiation medium [DM; Dulbecco's Modified Eagle's Medium (DMEM; Nacalai Tesque) containing 15% fetal bovine serum (FBS; Biofill), 100 μmol/L non-essential amino acids (NEAA; Invitrogen), 2 mmol/L L-glutamine (Invitrogen), and 0.1 mmol/L 2-mercaptoethanol (Invitrogen)] containing 0.2 μmol/L 6-bromoindirubin-3′-oxime (BIO; a glycogen synthase kinase-3β inhibitor, to activate the Wnt-signaling pathway) (Calbiochem), and cultured in 96-well Corning Costar Ultra-Low attachment multiwell plates (Sigma-Aldrich) for 3 days. On day 3, an additional 100 μL DM without BIO was added to each well. On day 5, individual embryoid bodies (EBs) were transferred to 100-mm gelatin-coated dishes (250 EBs per dish). On days 6, 7, 10, 11, 14, and 15 the medium was exchanged for serum-free Modified Eagle's Medium (MEM; Invitrogen) with insulin transferrin-selenium-X (Invitrogen). On days 8, 9, 12, and 13, the medium was exchanged for Glucose-free DMEM (no glucose, no pyruvate, Invitrogen) supplemented with 4 mmol/L lactic acid (Wako Pure Chemical) for purification of cardiomyocytes. On day 16, the contracting cell clusters were used as cardiomyogenically differentiated iPSCs (959A2-1 CMs, 959C1-1 CMs, 956F-1 CMs: iPSC-CMs). The protocol and purification process are illustrated in Figure 1a.

Adult cardiac tissue from B6 mice (CLEA) was used as a control. Male B6 mice (8 weeks old) were sacrificed by intravenous administration of potassium chloride under inhalation anesthesia of isoflurane, and heart tissue from the left ventricle was harvested for further studies and labeled "Heart".

Immunohistochemistry analysis

IPSC-CMs were dissociated with 0.25% trypsin-EDTA and then fixed with 4% paraformaldehyde. The cells were stained with the following primary antibodies: mouse anti-α-actinin antibody (Sigma-Aldrich) and rabbit anti-troponin I antibody (Abcam), and then visualized by the following secondary antibodies: Alexa Fluor 488 donkey anti-mouse IgG (Invitrogen) and Alexa Fluor 594 goat anti-rabbit IgG (Invitrogen). The nucleus of the cells were stained with 4′, 6-Diamidino-2-phenylindole dihydrochloride (DAPI) and then observed with a confocal laser scanning microscopy FV1200 (Olympus).

Ca^{2+} transient measurement and pharmacological analysis

5 μM Fluo-8 regents (AAT Bioquest, Inc.) in serum-free MEM was added to iPSC-CMs after the cells were washed with phosphate buffered saline. The cells were incubated at 37°C for 30 min and then observed with a fluorescence microscopy. Fluorescence intensity of Fluo-8 dye was sequentially measured using iQ2 software (ANDOR) pre and post the administration of 1 μM isoproterenol.

Flow cytometry

IPSC-CMs were dissociated with 0.25% trypsin-EDTA and then fixed with CytoFix fixation buffer (BD) for 20 min. The cells were permeabilized with Perm/Wash buffer (BD) at room temperature for 10 min and then incubated with mouse anti-troponin T antibody (Thermo) for 30 min. Cells were washed with Perm/Wash buffer prior to incubation with the Alexa Fluor 488 rabbit anti-mouse IgG secondary antibody (Invitrogen) at room temperature for 30 min. These cells were analyzed on a FACS Canto II (BD).

Characterization of *N*-glycans derived from iPSCs, iPSC-CM, and Heart

All experimental procedures, including chromatography conditions and glycosidase treatments, have been described previously [23]. Cultured undifferentiated iPSCs, iPSC-CMs, and the heart tissue were treated with chloroform–methanol, then subjected to proteolysis with chymotrypsin and trypsin, followed by glycoamidase A digestion to release *N*-glycans. After removal of peptides, the reducing ends of the *N*-glycans were derivatized with 2-aminopyridine (Wako). This mixture was applied to a diethylaminoethyl (DEAE) column (Tosoh) or a TSK-gel Amide-80 column (Tosoh); each fraction from the amide column was then applied to a Shim-pack HRC-octadecyl silane (ODS) column (Shimadzu). The elution times of individual peaks from the amide-silica and ODS columns were normalized to a pyridylamino (PA)-derivatized isomalto-oligosaccharide with a known degree of polymerization, and are represented as glucose units (GU). Thus, each compound from these two columns provided a unique set of GU values, which corresponded to the coordinates of the 2D HPLC map. The PA-oligosaccharides were identified by comparison to the coordinates of ~500 reference PA-oligosaccharides in a homemade web application, GALAXY (http://www.glycoanalysis.info/galaxy2/ENG/index.jsp) [24]. The calculated HPLC map based on the unit contribution values was used to estimate some high-mannose type PA-oligosaccharides. The PA-oligosaccharides were co-chromatographed with the reference to PA-oligosaccharides on the columns to confirm their identities. PA-glycans that did not correspond to any of the *N*-glycans registered in GALAXY were trimmed by exoglycosidase to produce a series of known glycans [25].

Mass spectrometry

PA-oligosaccharides were analyzed by matrix-assisted laser desorption/ionization time-of-flight mass spectrometric (MALDI-TOF/MS). The matrix solution was prepared as follows: 10 mg of 2,5-Dihydroxybenzoic acid (Sigma) was dissolved in 1:1 (v/v)

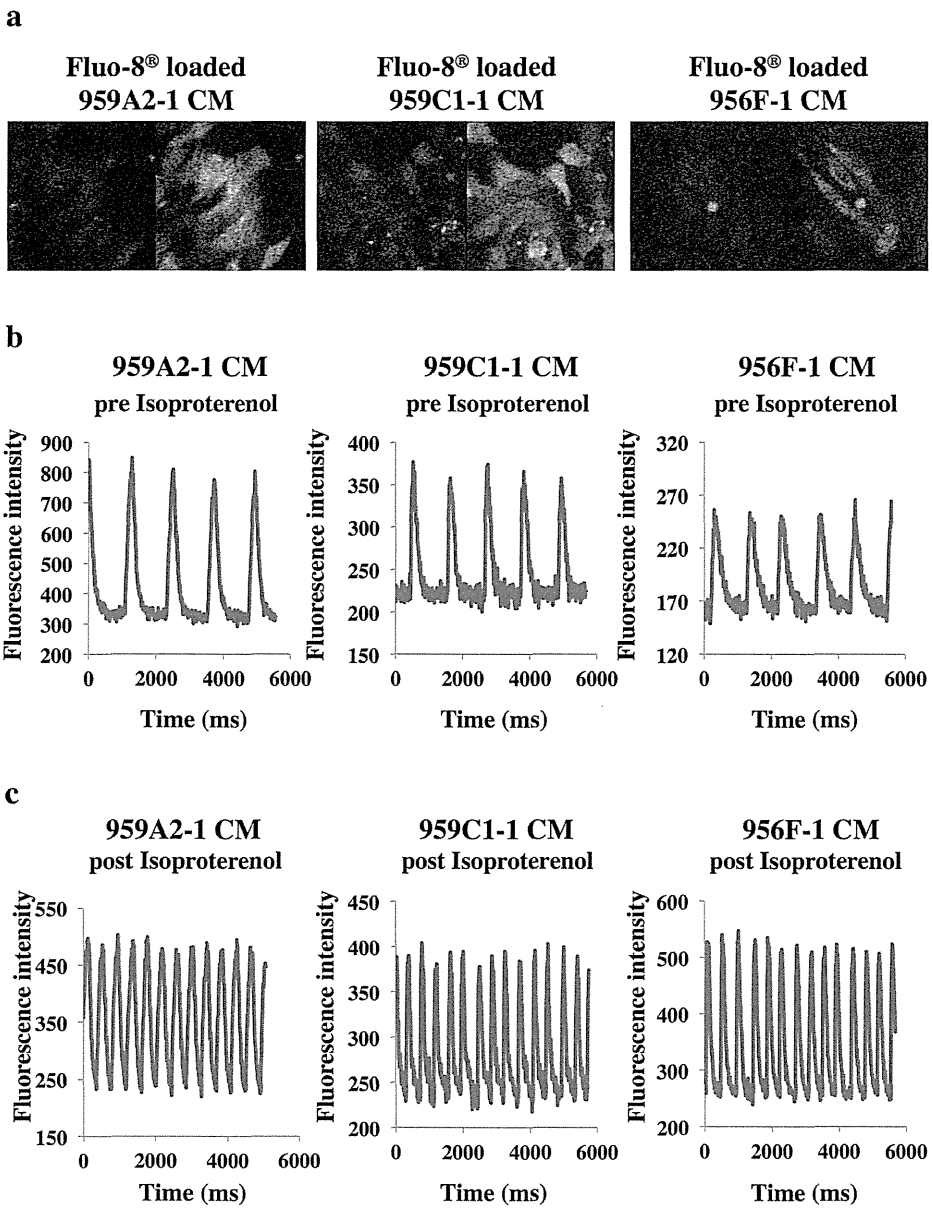

Figure 3. Ca^{2+} transient measurement of iPSC-CMs pre and post the administration of isoproterenol. (a) Fluo-8 loaded iPSC-CMs at the time of low (left) and high (right) fluorescence. (b), (c) Sequentially measured fluorescence intensity of Fluo-8 loaded iPSC-CMs pre (b) and post (c) the administration of 1 μM isoproterenol.
doi:10.1371/journal.pone.0111064.g003

acetonitrile/water (1 mL). Stock solutions of PA-glycans were prepared by dissolving them in pure water. One microliter of a sample solution was mixed on the target spot of a plate with 1 μL matrix solution and then allowed to air-dry. MALDI-TOF/MS data were acquired in the positive mode on an AXIMA-CFR (Shimadzu) operated in linear mode.

Materials

Glycoamidase A from sweet almond, α-mannosidase, β-galactosidase, and β-*N*-acetylhexosaminidase from jack bean were purchased from Seikagaku Kogyo (Tokyo, Japan). α-Galactosidase from coffee bean was purchased from Oxford GlycoSciences (Oxford, UK). Trypsin and chymotrypsin were obtained from Sigma (St. Louis, MO). Pronase protease from *Streptomyces griseus* was from Calbiochem (San Diego, CA). The pyridylamino (PA) derivatives of isomalto-oligosaccharides 4–20 (indicating the degree of polymerization of glucose residues) and reference PA-oligosaccharides were purchased from Seikagaku Kogyo.

Semi-quantitative PCR

DNA-free total RNA was extracted with the RNeasy RNA isolation Kit (Qiagen) and reverse-transcribed into cDNA using Omniscript reverse transcriptase (Qiagen), then analyzed by quantitative real-time PCR on an ABI PRISM 7700 thermocycler (Applied Biosystems) with the following TaqMan gene expression assays (Applied Biosystems): ST3Gal-III (Gal β1-3(4) GlcNAc α-2,

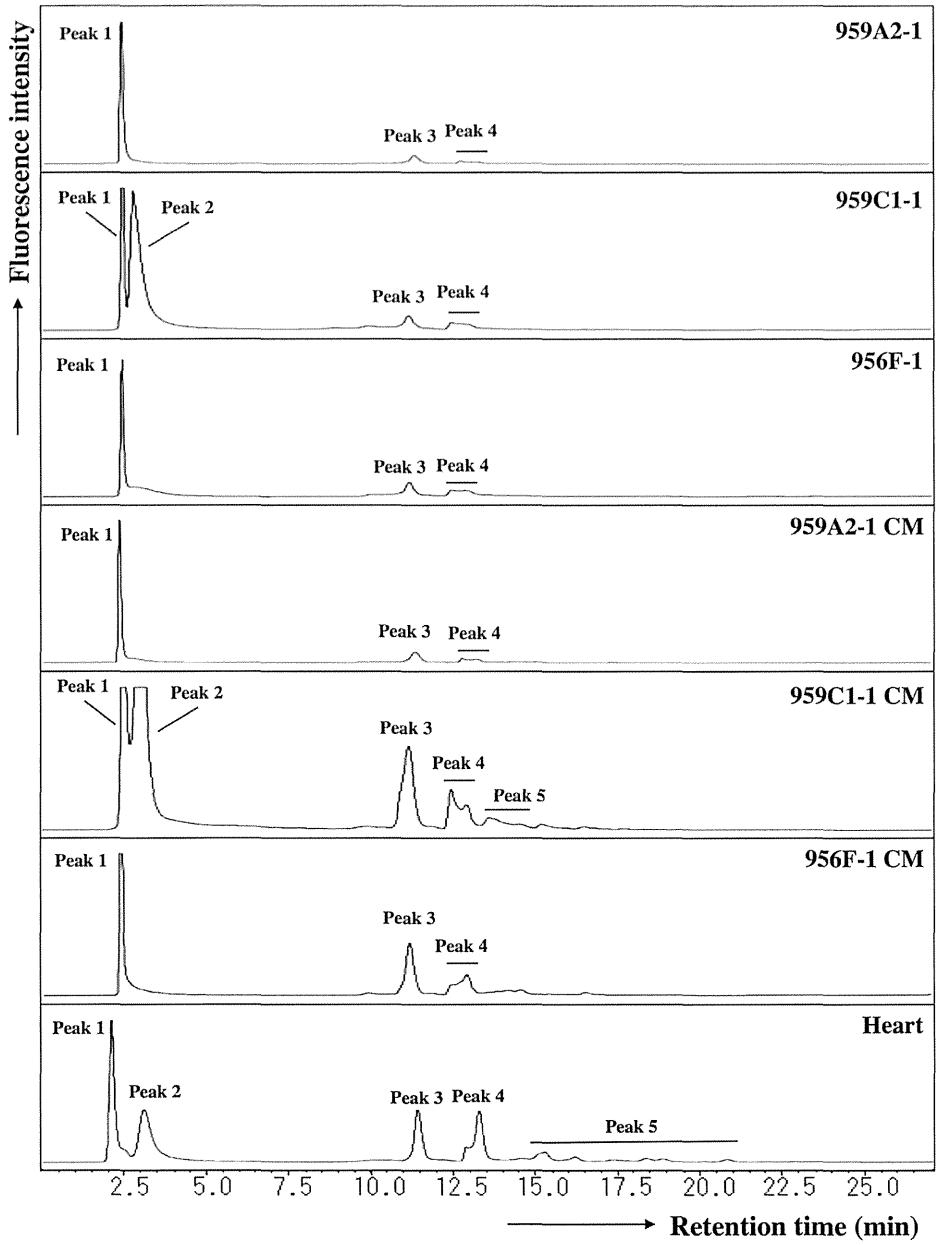

Figure 4. Anion-exchange DEAE elution profiles of PA-glycans. PA-glycans were fractionated according to their sialic acid content as neutral (peak 1), monosialyl (peak 3), and disialyl (peak 4) oligosaccharide fractions. Peaks 2 and 5 represent fractions containing no detectable PA-oligosaccharides.
doi:10.1371/journal.pone.0111064.g004

3-sialyltransferase), Mm00493353_m1; ST4Gal-IV (Gal β1-4(3) GlcNAc α-2, 3-sialyltransferase), Mm00501503_m1; ST6Gal-I (Gal β1-4 GlcNAc α-2, 6-sialyltransferase), Mm00486119_m1; CMAH (cytidine monophosphate-*N*-acetylneuraminic acid hydroxylase), Mm00483341_m1; GAPDH (glyceraldehyde-3-phosphate dehydrogenase), and Mm03302249_g1 and with SYBR Green dye (Applied Biosystems) using the following primers: Nkx2.5 F, 5′- CAAGTGCTCTCCTGCTTTCC -3′ R, 5′- GGCTTTGTCCAGCTCCACT -3′; αMHC (α-myosin heavy chain) F, 5′- GAGATTTCTCCAACCCAG -3′ R, 5′- TCTGACTTTCGGAGGTACT-3′; ANP (atrial natriuretic peptide) F, 5′-AAAGAAACCAGAGTGGGCAGAG -3′ R, 5′- CCAGGGTGATGGAGAAGGAG -3′; Isl1 F, 5′- TTTCCCTGTGTGTTGGTTGC -3′ R, 5′- TGATTACACTCCGCACATTTCA -3′; GAPDH F, 5′- CCAGTATGACTCCACTCACG -3′ R, 5′- GACTCCACGACATACTCAGC -3′. All experiments were performed by the relative standard curve method in three independent, triplicate experiments. Statistical comparison of the data was performed by Student's t-test.

Results

Highly purified cardiomyocytes derived from iPSCs

Cardiomyogenic differentiation was induced in murine iPSCs by using a slightly modified culture protocol (Figure 1a). The iPSC-CMs showed significantly higher expressions of Nkx2.5,

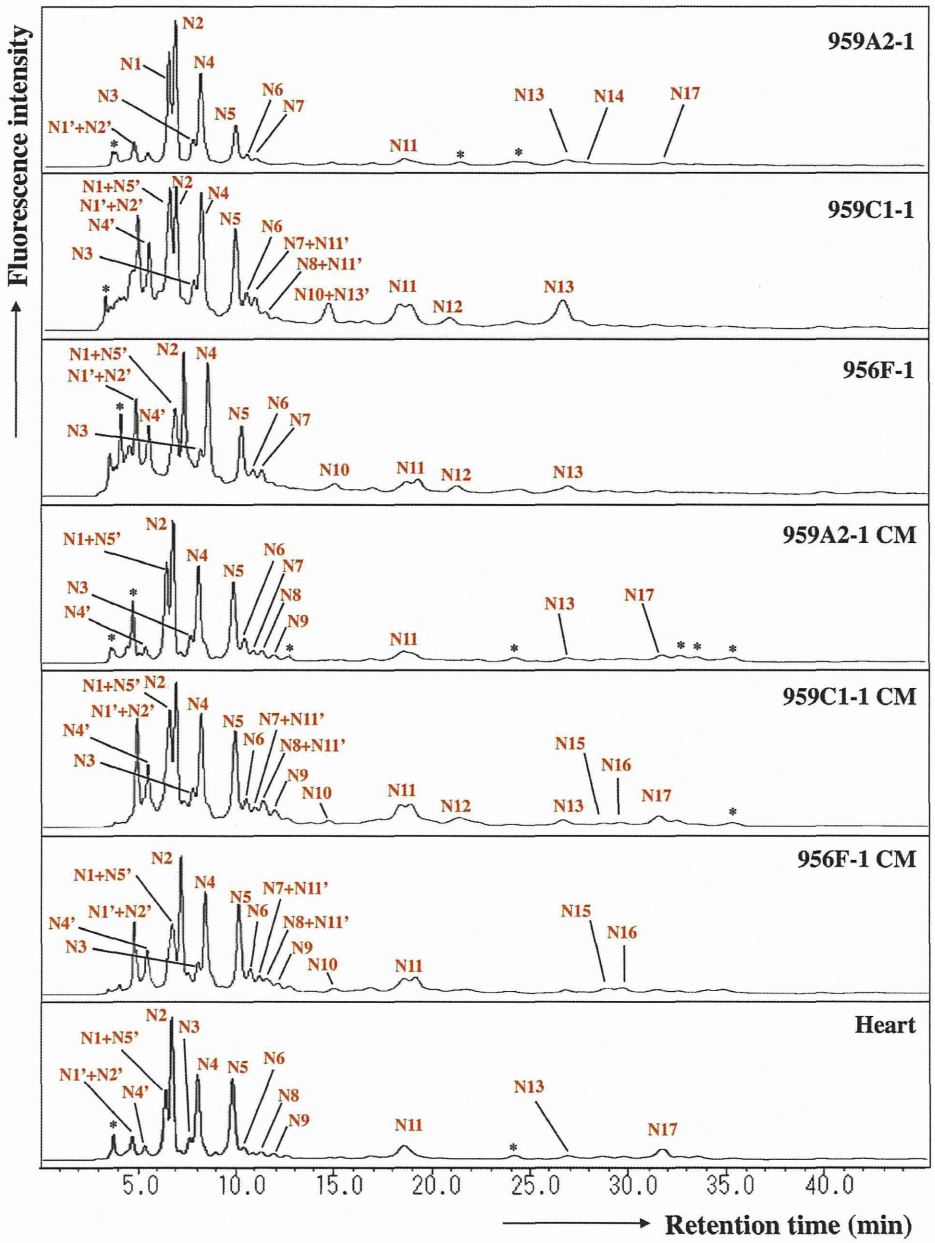

Figure 5. Reverse-phase ODS elution profiles of the neutral PA-glycans. The neutral fractions were individually applied to the ODS column and eluted according to their hydrophobicity. N1′, N2′, N4′, N5′ and N11′: epimerization of N1, N2, N4, N5 and N11. *Fractions containing no detectable PA-oligosaccharides.
doi:10.1371/journal.pone.0111064.g005

αMHC, ANP and Isl1 than undifferentiated iPSCs by semi-quantitative real-time PCR (Figure 2a), and showed sarcomere structures observed by immunohistological staining of α-actinin and troponin I (Figure 1b). The iPSC-CMs were functional with Ca^{2+} transient measurement (Figure 3a, b) and their beating rates were increased by the administration of isoproterenol (Figure 3c), meaning they had β-adrenergic receptors. Nearly all of the iPSC-CMs exhibited spontaneous and regular beating at room temperature (Video S1). The differentiation efficiency of murine iPSC was evaluated by flow cytometry analysis. More than 95% of the 959A2-1 CMs, 92% of the 959C1-1 CMs and 90% of the 956F-1 CMs were positive for troponin T (Figure 2b), while the undifferentiated iPSCs rarely expressed troponin T (Figure 2b).

N-Glycans isolated from iPSCs, iPSC-CM, and Heart

N-glycans extracted from undifferentiated iPSCs (959A2-1: 26 mg, 959C1-1: 11 mg and 956F-1: 10 mg of protein), iPSC-CM (959A2-1 CM: 15 mg, 959C1-1 CM: 12 mg and 956F-1 CM: 5.5 mg of protein), and the B6 heart muscle (82 mg of protein) were separated on a diethylaminoethyl (DEAE) column into five peaks, based on increasing acidity. Peak 1 represented a neutral (N) fraction, peak 3 a monosialyl (M) fraction, and peak 4 a disialyl

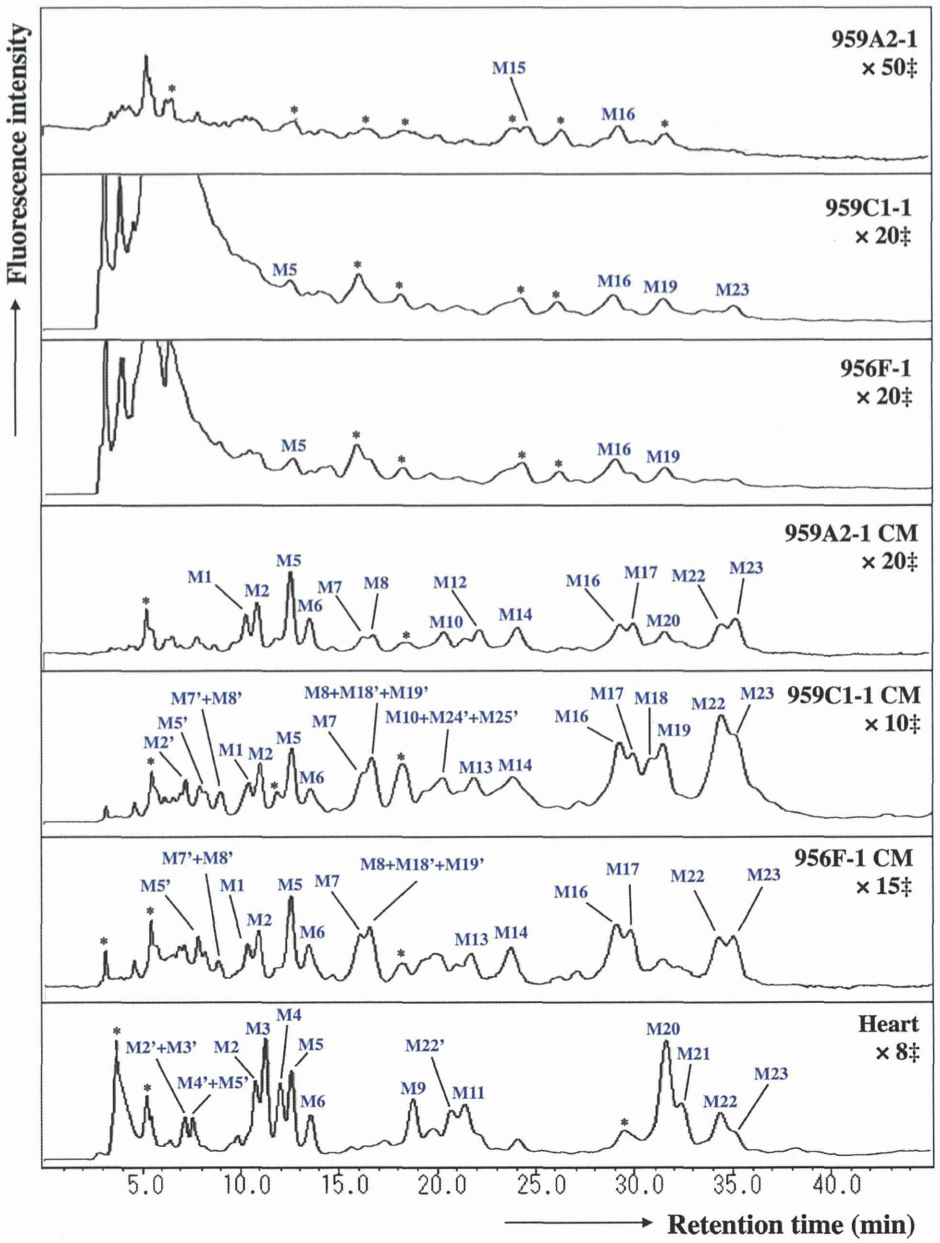

Figure 6. Reverse-phase ODS elution profiles of monosialyl PA-glycans. The monosialyl fractions were individually applied to the ODS column and eluted according to their hydrophobicity. M2′, M3′, M4′, M5′, M7′, M8′, M18′, M19′, M22′, M24′ and M25′: epimerization of M2, M3, M4, M5, M7, M8, M18, M19, M22, M24 and M25. *Fractions containing no detectable PA-oligosaccharides. ‡Magnification ratio to the fluorescence intensity of asialoglycan of each sample.
doi:10.1371/journal.pone.0111064.g006

(D) fraction. Glycan fractions in each of these peaks were as follows: iPSCs yielded 97% N, 0.5% M, 2.6% D (959A2-1), 98% N, 0.7% M, 1.1% D (959C1-1) and 96% N, 1.1% M, 3.1% D (956F-1) peak areas, iPSC-CMs yielded 89% N, 6.4% M, 4.4% D (959A2-1 CM), 79% N, 16% M, 4.8% D (959C1-1 CM) and 82% N, 10% M, 7.9% D (956F-1 CM) and Heart yielded 55% N, 19% M, and 25% D (Figure 4).

The ODS column separated the neutral fraction (Peak 1) into fractions N1–N17 (Figure 5), the monosialyl fraction (Peak 3) into fractions M1–M23 (Figure 6), and the disialyl fraction (Peak 4) into fractions D1–D12 (Figure 7). The signatures of each fraction differed between groups. These ODS fractions were individually fractionated on an amide column and analyzed by MALDI-TOF/MS. The N2, M6, M11, M14, M20, D4, D5, and D10 fractions contained two types of *N*-glycans, and the N6, N9, N11 and M2 fractions three types (data not shown). Thus, 68 different *N*-glycans were isolated from iPSCs, iPSC-CMs, and Heart.

Structures of *N*-Glycans isolated from iPSCs, iPSC-CM, and Heart

The isolated *N*-glycans were analyzed by means of a mapping technique based on their HPLC elution positions and MALDI-TOF/

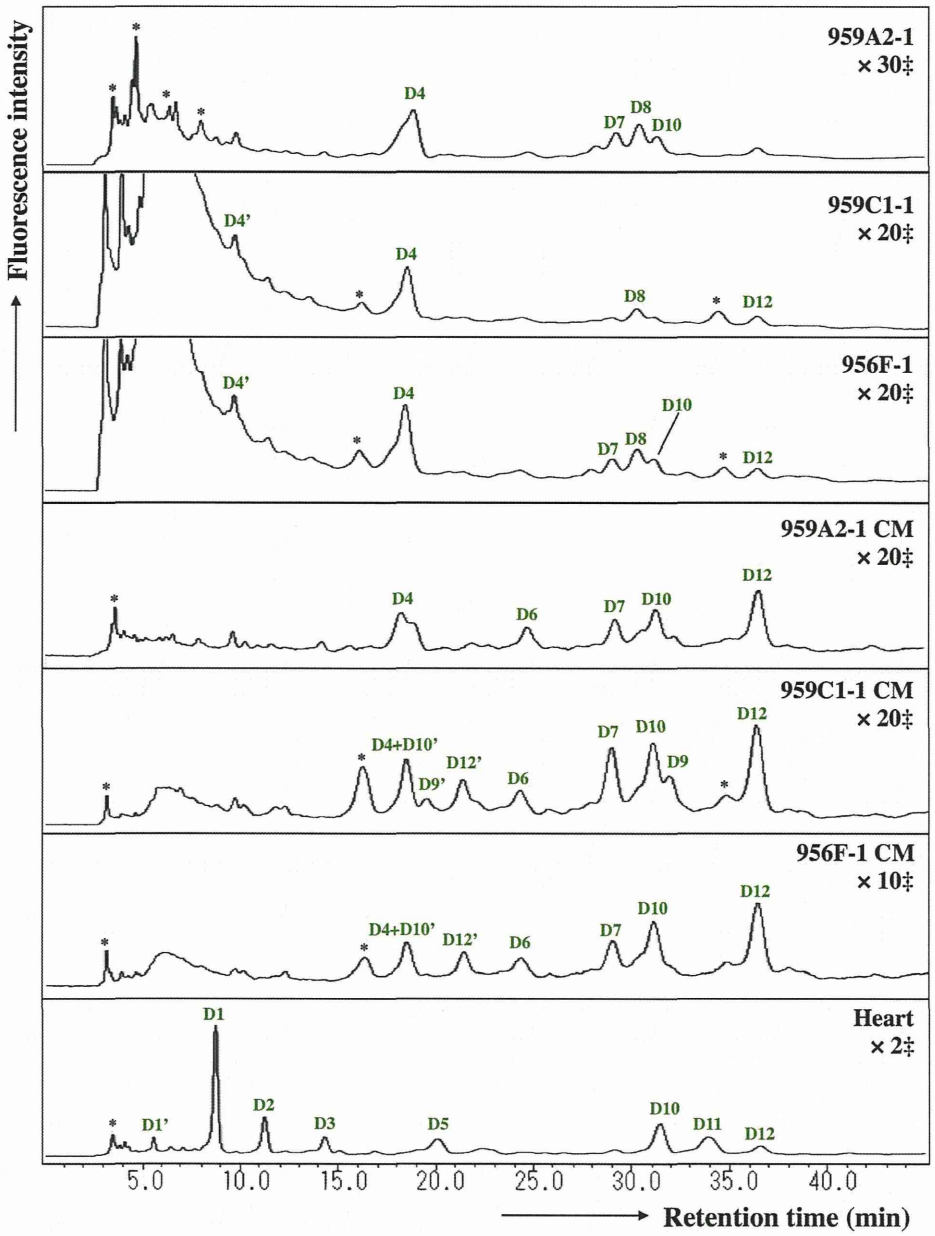

Figure 7. Reverse-phase ODS elution profiles of disialyl PA-glycans. The disialyl fractions were individually applied to the ODS column and eluted according to their hydrophobicity. D1′, D4′, D10′ and D12′: epimerization of D1, D4, D10 and D12; *Fractions containing no detectable PA-oligosaccharides. ‡Magnification ratio to the fluorescence intensity of asialoglycan of each sample.
doi:10.1371/journal.pone.0111064.g007

MS data. The coordinates of 54 *N*-glycans coincided with those for known references in the GALAXY database and their structures were identified. The coordinates for N9-3, M8, M11-2, M12, M13, M15, M17, M18, M19, M20-2, M21, M23, D8 and D9 did not correspond to known references.

N-glycans N9-2, M8, M12, M17, and M23 were trimmed by α-galactosidase but not by β-galactosidase or *N*-acetylglucosamidase. Their structures fit GALAXY references H5.12, 1A1-200.4, 1A3-200.4, 1A1-210.4, and 1A3-210.4, respectively. The galactosyl structures were then identified as Galα1-6Gal, because of the α-galactosidase-driven MS shifts. The structure of the M13 was identified by the coincidence with a GALAXY reference 1A2-H5.12 after being trimmed by α-L-fucosidase. The other *N*-glycans M11-2, M15, M18, M19, M20-2, M21, D8 and D9 were not identified in this study because they did not correspond to GALAXY references even after α-galactosidase digestions. They are described in Figure 8 and Table S1-S5 with their proposed formulas based on MALDI-TOF/MS data.

High-mannose *N*-Glycans were reduced by cardiomyogenic differentiation

The quantity of high-mannose *N*-glycans (HM) calculated from the total volume of N1–N6-2, N7 was highest in the iPSCs (959A2-1: 87.7%, 959C1-1: 68.3% and 956F-1: 78.2%), lower in the

Code No.	N1	N2-1	N2-2	N3	N4	N5	N6-1	N6-2	N6-3	N7	N8	N9-1
GU; ODS (Amid)	5.0 (8.8)	5.3 (7.9)	5.3 (9.5)	6.0 (7.8)	6.2 (7.0)	7.3 (6.0)	7.6 (4.2)	7.6 (5.0)	7.6 (4.6)	7.9 (3.3)	8.1 (7.3)	8.2 (5.6)
Mass (Da)	1800	1638	1962	1638	1475	1313	989	1151	1192	827	1679	1354
Structure	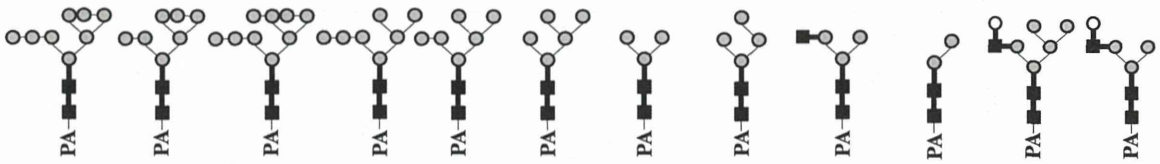											

N9-2	N9-3	N10	N11-1	N11-2	N11-3	N12	N13	N14	N15	N16	N17
8.2 (6.4)	8.3 (8.2)	9.3 (5.0)	10.5 (3.7)	10.5 (4.6)	10.5 (6.9)	11.2 (6.1)	12.8 (5.3)	13.0 (5.0)	13.3 (6.2)	13.5 (6.3)	14.2 (7.3)
1516	1841	1395	973	1135	1720	1500	1541	1338	1704	1704	1866
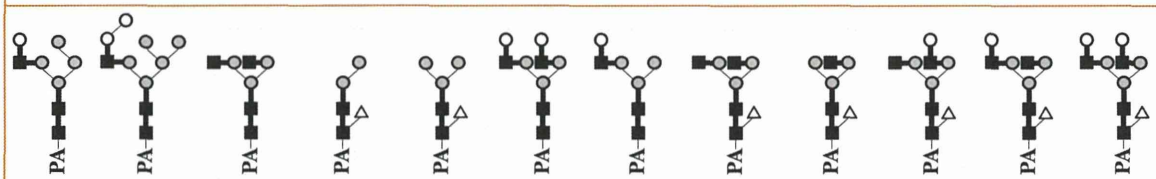											

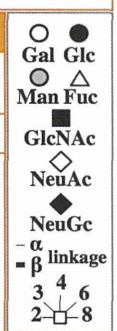

M1	M2-1	M2-2	M2-3	M3	M4	M5	M6-1	M6-2	M7	M8	M9	M10	M11-1	M11-2
7.6 (7.5)	7.9 (5.8)	7.9 (6.6)	7.9 (7.5)	8.1 (7.5)	8.4 (6.7)	8.6 (7.0)	9.0 (5.3)	9.0 (6.1)	10.1 (7.1)	10.3 (7.9)	10.6 (7.1)	11.0 (6.3)	11.3 (6.6)	11.3 (8.8)
1970	1646	1808	2027	1986	1824	1970	1646	1808	2011	2173	2027	1792	2011	2360
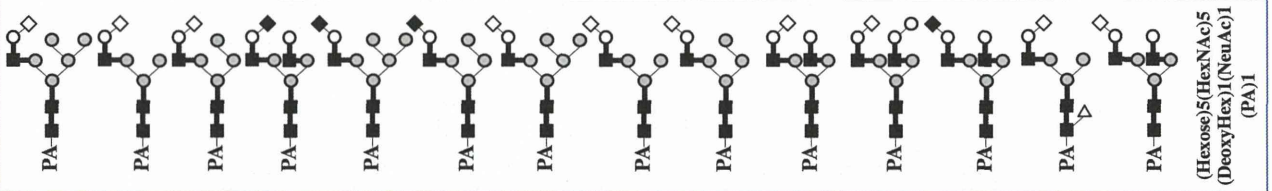														

M12	M13	M14-1	M14-2	M15	M16	M17	M18	M19	M20-1	M20-2	M21	M22	M23
11.5 (7.4)	11.3 (7.4)	11.8 (6.5)	11.8 (5.6)	12.1 (8.3)	13.3 (7.5)	13.7 (8.3)	13.8 (7.4)	14.0 (8.2)	14.2 (7.5)	14.2 (8.2)	14.5 (8.3)	15.1 (6.9)	15.3 (7.8)
2173	2116	1954	1792	2173	2157	2320	2360	2522	2173	2522	2344	2157	2320
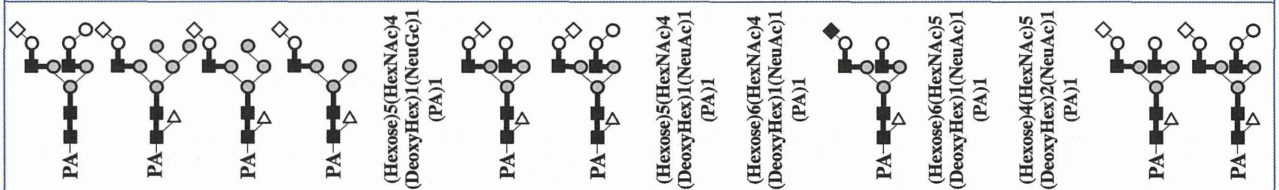													

D1	D2	D3	D4-1	D4-2	D5-1	D5-2	D6	D7	D8	D9	D10-1	D10-2	D11	D12
7.0 (8.2)	8.3 (7.8)	9.3 (8.6)	10.6 (6.9)	10.6 (7.3)	10.9 (7.4)	10.9 (8.1)	12.1 (6.4)	13.5 (7.7)	13.9 (6.8)	14.1 (7.5)	14.2 (7.2)	14.2 (7.7)	15.0 (7.2)	15.9 (6.7)
2334	2334	2480	2302	2302	2334	2480	2302	2448	2537	2854	2448	2480	2464	2448
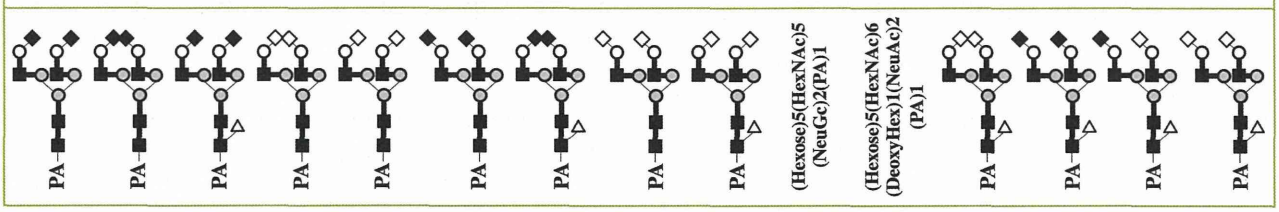														

Figure 8. Structures of neutral, monosialyl, and disialyl PA-oligosaccharides in iPSCs, iPSC-CM, and heart cells. Glucose units (GU) were calculated from the peak elution times for the ODS column in Figure 5, 6 and 7, and the amide column (data not shown). Average mass (Mass) calculated from the *m/z* values of $[M+Na]^+$ or $[M+H]^+$ ion for neutral, $[M-H]^-$ ion for monosialyl, and $[M-H]^-$ & $[M+Na-2H]^-$ ions for disialyl PA-oligosaccharides.
doi:10.1371/journal.pone.0111064.g008

iPSC-CMs (959A2-1 CM: 77.4%, 959C1-1 CM: 60.0% and 956F-1 CM: 65.1%), and lowest in the Heart (46.9%). The quantity of monofucosylated, difucosylated, and other types of *N*-glycans were greater in the iPSC-CMs and Heart (Figure 8, 9).

Sialyl *N*-glycans increased with cardiomyogenic differentiation

The quantity of monosialyl *N*-glycans (MS) calculated from the total volume of M1–M23 increased in iPSC-CMs (959A2-1 CM: 6.4%, 959C1-1 CM: 15.7% and 956F-1 CM: 10.5%) and Heart (19%) and were low in iPSCs (959A2-1: 0.5%, 959C1-1: 0.7% and 956F-1: 1.1%). The disialyl *N*-glycans (DS; D1–D12) yielded a similar pattern. The quantity of asialyl *N*-glycans (AS; N1–N17) decreased in iPSC-CMs (959A2-1 CM: 89.2%, 959C1-1 CM: 79.4% and 956F-1 CM: 81.7%) and Heart (55.3%) in comparison to the iPSCs (959A2-1: 96.9%, 959C1-1: 98.1% and 956F-1: 95.8%) (Figure 9, 10).

Rarely expressed *N*-glycans

The sialic acids identified in this study were either *N*-acetyl neuraminic acid (NeuAc) or *N*-glycolyl neuraminic acid (NeuGc). The quantity of monosialyl and disialyl *N*-glycans containing only NeuAc (A, A/A) was lowest in iPSCs (959A2-1: 2.5%, 959C1-1: 1.7% and 956F-1: 3.7%) and similar in iPSC-CMs (959A2-1 CM: 10.6%, 959C1-1 CM: 21% and 956F-1 CM: 18%) and the Heart (8%). The quantity of monosialyl and disialyl *N*-glycans containing only NeuGc (G, G/G) was markedly higher in the Heart (32.8%) than in iPSCs (959A2-1: 0.6%, 959C1-1: 0.1% and 956F-1: 0.5%) or iPSC-CMs (959A2-1 CM: 0%, 959C1-1 CM: 0% and 956F-1 CM: 0%) (Figure 10a).

Expression of glycosyl transferase, ST3Gal-III, ST3Gal-IV, ST6Gal-I, and CMAH in the iPSCs, iPSC-CMs, and Heart was assessed by RT-PCR to explore the glycan structures responsible for the differences between groups. The Heart expressed high levels of CMAH (0.91±0.13/GAPDH); levels in the iPSCs and iPSC-CMs were markedly lower (iPSCs: 959A2-1 0.011±0.0065/GAPDH, 959C1-1 0.013±0.0070/GAPDH, 956F-1 0.0045±0.0042/GAPDH, $P<0.05$; iPSC-CM: 959A2-1 CM 0.21±0.16/GAPDH, 959C1-1 CM 0.19±0.04, 956F-1 CM 0.45±0.31, $P<0.05$). Expression of ST3Gal-III was significantly higher in the Heart (0.98±0.13/GAPDH) than in iPSCs (959A2-1: 0.21±0.05/GAPDH, 959C1-1: 0.18±0.07/GAPDH, 956F-1: 0.27±0.05/GAPDH) and iPSC-CMs (959A2-1 CM: 0.40±0.10/GAPDH, 959C1-1 CM: 0.35±0.09/GAPDH, 956F-1 CM: 0.66±0.18); expression of ST3Gal-IV did not differ between groups. ST6Gal-I expression was significantly higher in iPSC-CMs (959A2-1 CM: 1.87±0.41/GAPDH, 959C1-1 CM: 1.95±0.22/GAPDH, 956F-1 CM: 3.08±1.27/GAPDH) than in iPSCs (959A2-1: 0.51±0.18/GAPDH, 959C1-1: 0.40±0.09/GAPDH, 956F-1: 0.62±0.29/GAPDH) and the Heart (1.04±0.13/GAPDH) (Figure 10b).

Discussion

Sixty-eight different *N*-glycans were isolated from iPSCs, iPSC-CMs, and the Heart. The structures of 60 *N*-glycans were identified, based on their HPLC elution peaks (Figure 8, Table S1-S5). Each preparation contained a combination of neutral, monosialyl, and disialyl *N*-glycans.

The molar ratios of high-mannose, monofucosylated, and difucosylated *N*-glycans were substantially different between groups (Figure 9), although no clear differences in the abundance of these glycans were found. The decrease in high-mannose *N*-glycans and increase of fucosylated *N*-glycans in iPSC-CMs versus iPSCs is consistent with a previous report on a comparison of ESC derived cardiomyocytes to undifferentiated ESCs [18]. Generally, all *N*-glycans are synthesized from the high-mannose type by a large array of sequentially and competitively acting biosynthetic enzymes located throughout the endoplasmic reticulum and Golgi apparatus [26], indicating that the high-mannose type of *N*-glycans could be categorized as a marker of immaturity. In this study, the high-mannose *N*-glycans were highest in the immature iPSC and lowest in the Heart, or mature tissue; thus, the quantity of high-mannose-type *N*-glycans might be an indicator of maturity in iPSC-derivatives and the iPSC-CMs in our protocol may still be immature in comparison to cardiac tissue.

Clear differences in glycan abundance were observed, such as hybrid and complex types represented by N9-1, N9-3, N15, N16, M1, M2-1, M2-2, M7, M8, M10, M12, M13, M14-1, M14-2, M17, M18, M20-2, D6 and D9 in iPSC-CMs, M2-3, M3, M4, M9, M11-1, M11-2, M20-1, M21, D1, D2, D3, D5-1, D5-2, D10-2 and D11 in Heart and N14 and M15 in iPSCs; these may also be indicators of maturation stage. In addition, expression of monosialyl and disialyl *N*-glycans in iPSC-CMs fell between the levels observed in the iPSCs and Heart, as were the molar ratios, indicating that the iPSC-CMs may still be immature stage. While many *N*-glycolyl neuraminic acid (NeuGc) structures were detected in the Heart, iPSCs and iPSC-CMs did not contain NeuGc in their sialyl structures, except for D8. Moreover, the molar ratio of NeuAc was low in iPSCs and iPSC-CMs. This finding is one of the clearest differences between iPSCs or iPSC-CMs and Heart cells.

The proposed spectra-based composition of the D8 glycans in iPSCs was [(Hexose)5(HexNAc)5(NeuGc)2(PA)1], indicating that it contains NeuGc. However, D8 might be quite a rare exception because transcript levels of CMAH, which catalyzes the conversion of NeuAc to NeuGc, was quite low in iPSCs in comparison to the Heart. This data suggests that during the process of reprograming, iPSCs suppress or eliminate CMAH activity. We conclude that iPSCs contain less sialic acid (especially NeuGc) and high-mannose structures are abundant in the *N*-glycans. In contrast, heart cells produce numerous sialyl-*N*-glycans, especially NeuGc. Transcript levels of CMAH tended to increase in iPSC-CMs relative to iPSCs, suggesting cardiomyogenic differentiation may induce expression of CMAH. If the iPSC-CMs could be matured more closely to the Heart by some additional methods of culture, the quantity of high mannose type of *N*-glycans might decrease more closely to the Heart, and might produce *N*-glycans containing NeuGc, followed by the expression of CMAH.

A terminal NeuGc, the Hanganutziu-Deicher (H-D) epitope [27], is widely distributed in the animal kingdom with the exception of humans and chickens. Expression of NeuGc is controlled by CMAH activity. Irie et al. [28] and Chou et al. [29] cloned the cDNA for human CMAH and reported that the *N*-terminal truncation of human CMAH is caused by deletion of Exon 6, a 92-base pair segment in the genomic DNA. Expression of this truncation in the heart eliminates NeuGc in sialyl

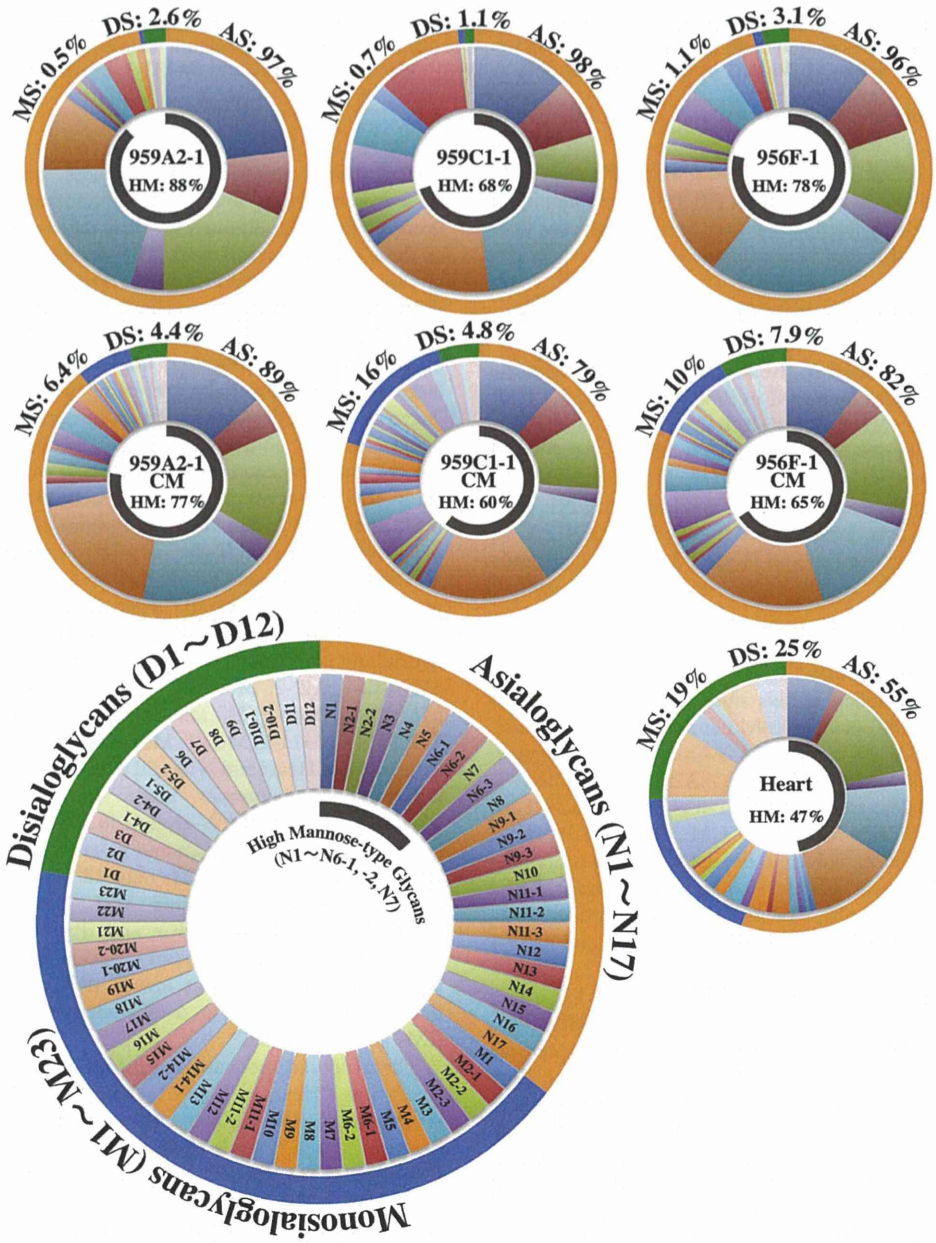

Figure 9. Relative quantities of neutral, monosialyl, and disialyl PA-oligosaccharides in iPSCs, iPSC-CM, and heart cells. Relative quantities of each glycan, calculated from the peak area in Figure 5, 6 and 7 vs. total *N*-glycan content in each cell, were expressed in the doughnut charts. Relative quantities of the asialoglycans, the monosialoglycans and the disialoglycans were showed outside of the charts, and relative quantities of the high mannose type glycans were showed inside of the charts. Asialoglycan (AS): the total volume of N1-N17; Monosialoglycan (MS): the total volume of M1-M23; Disialoglycan (DS): the total volume of D1-D12, High mannose-type glycan (HM): the total volume of N1–N6-1, N6-2, N7.
doi:10.1371/journal.pone.0111064.g009

structures. If human iPSCs or iPSC-CMs do not express CMAH in the same way as murine iPSCs or iPSC-CMs, there may be no difference between human iPSCs, iPSC-CMs, and the human Heart. Further study on human iPSC-CM will be needed to completely understand the features of the sialyl acid of *N*-glycans.

It was reported that human iPSCs produced α2,6sialyl glycans but did not contain α2,3sialyl structures, in contrast to human fibroblast, the origin of iPSCs, which produced α2,3sialyl but not α2,6sialyl structures [30,31]. The murine iPSCs in this study contained α2,3sialyl structures in NeuAc, M5, M23, D4-1, D10-1 and D12, and the iPSC-CMs produced α2,3 and α2,6sialyl structures in NeuAc. These differences may be due to variations between species, because mouse Heart cells also contained α2,3 and α2,6sialyl structures in NeuGc. Further studies are needed to characterize the glycome shift in the production and differentiation of iPSCs.

Type I Lactose structures were not detected, although over 98% of glycans in each cell were accounted for in this study. The *N*-glycans of N9-3, M8, M12, M17, and M23, which were identified after α-galactosidase digestion, contained Galα1-6Gal, not only in

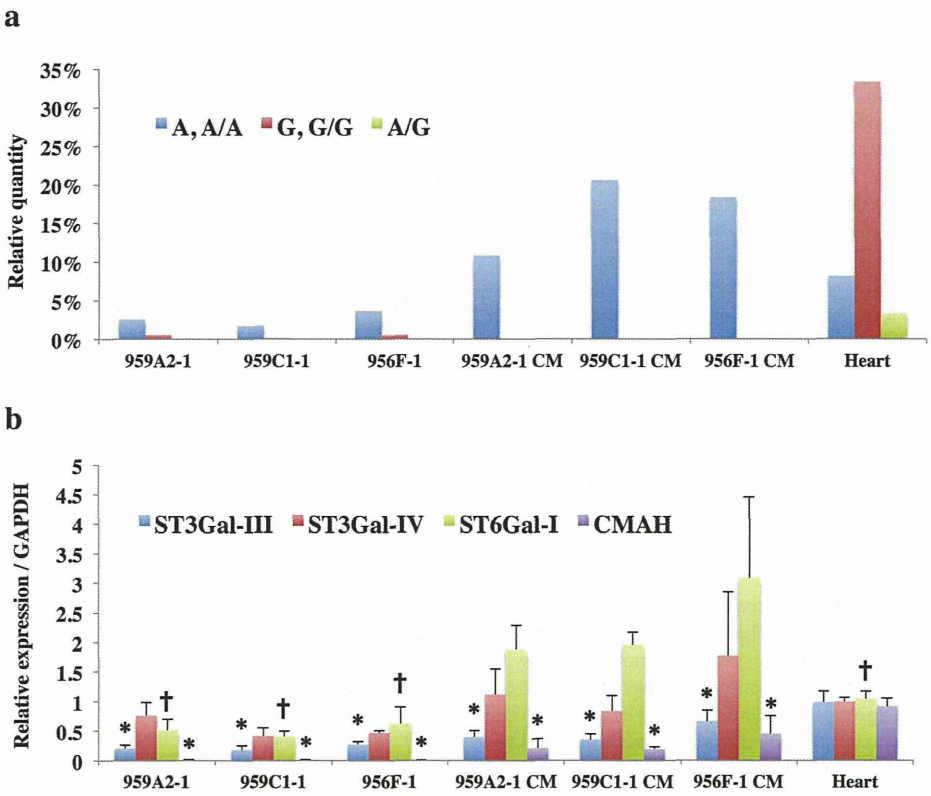

Figure 10. Rarely expressed NeuGc-containing glycans in iPSCs and iPSC-CMs. (a) Relative quantities of NeuAc- and NeuGc-containing glycans; Monosialoglycans containing NeuAc and Disialoglycans containing two NeuAc (A, A/A): the total volume of M1, M2-1, M2-2, M5-M8, M10-M14, M16-M19, M20-2, M21-M23, D4-1, D4-2, D6, D7, D9, D10-1, D12, Disialoglycan containing NeuAc and NeuGc (A/G): D11, Monosialoglycan containing NeuGc and Disialoglycan containing two NeuGc (G, G/G): the total volume of M2-3, M3, M4, M9, M15, M20-1, D1-D3, D5-1, D5-2, D8, D10-2. (b) Transcript expression of ST3Gal-III, ST3Gal-IV, ST6Gal-I, and CMAH; Transcript expression of glycosyltransferases in iPSCs, iPSC-CM, and heart cells was analyzed by real-time PCR. Results are expressed as the mean ± standard deviation. *P<0.05 vs. Heart, †P<0.05 vs. iPSC-CM (all of the 959A2-1 CM, 959C1-1 CM and 956F-1 CM).
doi:10.1371/journal.pone.0111064.g010

the neutral glycans but also in the monosialyl *N*-glycans of the iPSC-CM preparation. The same structure was not found in iPSCs, but only one structure, M23, was present in Heart cells. Therefore, in iPSC-CMs, Galα1-6Gal enzyme activity appears to be up-regulated in comparison to wild-type myocardium, although enzyme activity was not assessed by RT-PCR because of the limited availability of genetic sequence data.

The D8 was identified in all of three iPSC lines and not in the iPSC-CMs and Heart. This structure, unfortunately not identified in this study, may be useful as markers of undifferentiated iPSCs in the same way as well-known pluripotency biomarkers such as stage-specific embryonic antigens (SSEA)-3, SSEA-4 (glycosphingolipids) [32].

Previous MALDI-TOF/MS and MS/MS studies concluded that many kinds of *N*-glycans are found in organs and cells. The number of detected *N*-glycans is attributed to the sensitivity of the MS and HPLC methods employed. That is, MS data are sensitive and can be rapidly obtained, but a glycan structure is identified based only on the calculated molecular weight. Therefore, discriminating between isomeric structures is difficult. On the other hand, it thus appears that the accuracy of the data presented here using HPLC mapping in conjunction with a MALDI-TOF technique provides much more detailed information. Our data were used to identify the representative features of each *N*-glycan in these three cell types.

There may be a concern that the heart tissue used in this study contains connective tissues, vessels or nerves other than cardiomyocytes. Therefore, some of the *N*-glycans detected from the Heart sample might be derived from the tissues other than cardiomyocytes. However, heart is majority composed by cardiomyocytes, and furthermore, even if a small amount of *N*-glycans derived from connective tissues were contaminated in the Heart sample, the main evidences in this study, such as the proportion of the high-mannose type *N*-glycans, the ratio of the active sialyltransferase genes, the existence of NeuGc, and the uncommonness of Galα1-6 Gal, are essentially not affected.

In summary, murine iPSCs were rich in high-mannose type *N*-glycans but very poor in sialyl type *N*-glycans. Murine heart tissue contained a relatively low volume of high-mannose glycans, but was very rich in neuraminic acid, especially NeuGc type sialyl structures. Under these conditions, the volume of each type of glycan was similar for iPSC-CMs and iPSCs. That is, they were rich in high-mannose and relatively poor in sialyl type *N*-glycans by volume. In addition, most of the sialyl structures of the iPSC-CMs were different from those of the Heart, and the iPSC-CMs expressed no NeuGc. Moreover, the iPSC-CMs produced several unique glycans with the Galα1-6Gal structure. These results

provide important data that can be useful in future clinical iPSC studies.

It is quite important to investigate the meaning of *N*-glycans transitions during the cardiomyogenic differentiation presented in this study, for deeply understanding the relationship between the *N*-glycan expression and cardiomyogenic differentiation. Knock-out or knock-down of the genes related to cardiomyogenic differentiation or glycosylation may be useful for such purpose. However, the *N*-glycan signature in the cell surface is determined by a variety of the genes. Knock-out or knock-down of a single gene related to cardiomyogenic differentiation would alter an array of gene expressions, such as sarcomere proteins, transcriptional factors, or cell surface proteins, all of which would affect the signature of *N*-glycans in the cell surface. Therefore, the data interpretation for relationship between expression of a single gene and *N*-glycan signature would be difficult. Some different experimental approach may be needed to investigate the meaning of change in *N*-glycan expression during cardiomyogenic differentiation.

Supporting Information

Table S1 Structures and relative quantities of neutral (Table S1, S2) PA-oligosaccharides derived from iPSC, iPSC-CM, and heart cells. a. Glucose units (GU) were calculated from the peak elution times of the peaks obtained from the ODS column in Figure 5, 6, 7 and the Amide column (data not shown). b. Average mass calculated from the *m/z* values of $[M+Na]^+$ or $[M+H]^+$ ion for neutral, $[M-H]^-$ ion for mono-sialyl, and $[M-H]^-$ & $[M+Na-2H]^-$ ions for di-sialyl PA-oligosaccharides. c. PA-oligosaccharide structures. d. mol% was calculated from the peak area versus total *N*-glycan content in each cell
(TIFF)

Table S2 Structures and relative quantities of neutral (Table S1, S2) PA-oligosaccharides derived from iPSC, iPSC-CM, and heart cells.
(TIFF)

Table S3 Structures and relative quantities of mono-sialyl (Table S3, S4) PA-oligosaccharides derived from iPSC, iPSC-CM, and heart cells.
(TIFF)

Table S4 Structures and relative quantities of mono-sialyl (Table S3, S4) PA-oligosaccharides derived from iPSC, iPSC-CM, and heart cells.
(TIFF)

Table S5 Structures and relative quantities of disialyl PA-oligosaccharides derived from iPSC, iPSC-CM, and heart cells.
(TIFF)

Video S1
(MP4)

Acknowledgments

Our deepest appreciation goes to Professor Shinya Yamanaka and Keisuke Okita of the Center for iPS Cell Research and Application, Kyoto University, who kindly provided the murine iPSCs. We also thank Sachiko Kondo and Uichiro Yabe of MBL, Nagoya, Japan, who gave invaluable comments regarding *N*-glycan analysis.

Author Contributions

Conceived and designed the experiments: TK S. Miyagawa S. Miyagawa JL YS. Performed the experiments: TK AY NK AK EI AM HE KT. Analyzed the data: TK S. Miyagawa YS. Contributed reagents/materials/analysis tools: TK AY JL. Wrote the paper: TK S. Miyagawa YS SF. Obtained permission for use of cell line: S. Miyagawa AS YS.

References

1. Gonzales C, Pedrazzini T (2009) Progenitor cell therapy for heart disease. Exp Cell Res 315: 3077–3085.
2. Shah AM, Mann DL (2011) In search of new therapeutic targets and strategies for heart failure: recent advances in basic science. Lancet 378: 704–712.
3. Yoshida Y, Yamanaka S (2010) Recent stem cell advances: induced pluripotent stem cells for disease modeling and stem cell-based regeneration. Circulation 122: 80–87.
4. Yoshida Y, Yamanaka S (2011) iPS cells: A source of cardiac regeneration. Journal of Molecular and Cellular Cardiology 50: 327–332.
5. Kawamura M, Miyagawa S, Miki K, Saito A, Fukushima S, et al. (2012) Feasibility, safety, and therapeutic efficacy of human induced pluripotent stem cell-derived cardiomyocyte sheets in a porcine ischemic cardiomyopathy model. Circulation 126: S29–37.
6. Mercola M, Colas A, Willems E (2013) Induced pluripotent stem cells in cardiovascular drug discovery. Circ Res 112: 534–548.
7. Sinnecker D, Goedel A, Laugwitz KL, Moretti A (2013) Induced pluripotent stem cell-derived cardiomyocytes: a versatile tool for arrhythmia research. Circ Res 112: 961–968.
8. Kamakura T, Makiyama T, Sasaki K, Yoshida Y, Wuriyanghai Y, et al. (2013) Ultrastructural maturation of human-induced pluripotent stem cell-derived cardiomyocytes in a long-term culture. Circ J 77: 1307–1314.
9. Kuzmenkin A, Liang H, Xu G, Pfannkuche K, Eichhorn H, et al. (2009) Functional characterization of cardiomyocytes derived from murine induced pluripotent stem cells in vitro. FASEB J 23: 4168–4180.
10. Varki A (1993) Biological roles of oligosaccharides: all of the theories are correct. Glycobiology 3: 97–130.
11. Haltiwanger RS, Lowe JB (2004) Role of glycosylation in development. Annu Rev Biochem 73: 491–537.
12. Ohtsubo K, Marth JD (2006) Glycosylation in cellular mechanisms of health and disease. Cell 126: 855–867.
13. Surani MA (1979) Glycoprotein synthesis and inhibition of glycosylation by tunicamycin in preimplantation mouse embryos: compaction and trophoblast adhesion. Cell 18: 217–227.
14. Akama TO, Nakagawa H, Sugihara K, Narisawa S, Ohyama C, et al. (2002) Germ cell survival through carbohydrate-mediated interaction with Sertoli cells. Science 295: 124–127.
15. Hato M, Nakagawa H, Kurogochi M, Akama TO, Marth JD, et al. (2006) Unusual N-glycan structures in alpha-mannosidase II/IIx double null embryos identified by a systematic glycomics approach based on two-dimensional LC mapping and matrix-dependent selective fragmentation method in MALDI-TOF/TOF mass spectrometry. Mol Cell Proteomics 5: 2146–2157.
16. Lau KS, Partridge EA, Grigorian A, Silvescu CI, Reinhold VN, et al. (2007) Complex N-glycan number and degree of branching cooperate to regulate cell proliferation and differentiation. Cell 129: 123–134.
17. Kraushaar DC, Rai S, Condac E, Nairn A, Zhang S, et al. (2012) Heparan sulfate facilitates FGF and BMP signaling to drive mesoderm differentiation of mouse embryonic stem cells. J Biol Chem 287: 22691–22700.
18. Amano M, Yamaguchi M, Takegawa Y, Yamashita T, Terashima M, et al. (2010) Threshold in stage-specific embryonic glycotypes uncovered by a full portrait of dynamic N-glycan expression during cell differentiation. Mol Cell Proteomics 9: 523–537.
19. Okita K, Nakagawa M, Hyenjong H, Ichisaka T, Yamanaka S (2008) Generation of mouse induced pluripotent stem cells without viral vectors. Science 322: 949–953.
20. Miki K, Uenaka H, Saito A, Miyagawa S, Sakaguchi T, et al. (2012) Bioengineered myocardium derived from induced pluripotent stem cells improves cardiac function and attenuates cardiac remodeling following chronic myocardial infarction in rats. Stem Cells Transl Med 1: 430–437.
21. Yu T, Miyagawa S, Miki K, Saito A, Fukushima S, et al. (2013) In vivo differentiation of induced pluripotent stem cell-derived cardiomyocytes. Circ J 77: 1297–1306.
22. Tohyama S, Hattori F, Sano M, Hishiki T, Nagahata Y, et al. (2013) Distinct metabolic flow enables large-scale purification of mouse and human pluripotent stem cell-derived cardiomyocytes. Cell Stem Cell 12: 127–137.
23. Takahashi N, Khoo KH, Suzuki N, Johnson JR, Lee YC (2001) N-glycan structures from the major glycoproteins of pigeon egg white: predominance of terminal Galalpha(1)Gal. J Biol Chem 276: 23230–23239.

24. Takahashi N, Kato K (2003) GALAXY(Glycoanalysis by the Three Axes of MS and Chromatography): a Web Application that Assists Structural Analyses of N-Glycans. Trends in Glycoscience and Glycotechnology 15 No.84: 235–251.
25. Yagi H, Takahashi N, Yamaguchi Y, Kimura N, Uchimura K, et al. (2005) Development of structural analysis of sulfated N-glycans by multidimensional high performance liquid chromatography mapping methods. Glycobiology 15: 1051–1060.
26. Dalziel M, Crispin M, Scanlan CN, Zitzmann N, Dwek RA (2014) Emerging principles for the therapeutic exploitation of glycosylation. Science 343: 1235681.
27. Varki A (2009) Multiple changes in sialic acid biology during human evolution. Glycoconj J 26: 231–245.
28. Irie A, Koyama S, Kozutsumi Y, Kawasaki T, Suzuki A (1998) The molecular basis for the absence of N-glycolylneuraminic acid in humans. J Biol Chem 273: 15866–15871.
29. Chou HH, Takematsu H, Diaz S, Iber J, Nickerson E, et al. (1998) A mutation in human CMP-sialic acid hydroxylase occurred after the Homo-Pan divergence. Proc Natl Acad Sci U S A 95: 11751–11756.
30. Hasehira K, Tateno H, Onuma Y, Ito Y, Asashima M, et al. (2012) Structural and quantitative evidence for dynamic glycome shift on production of induced pluripotent stem cells. Mol Cell Proteomics 11: 1913–1923.
31. Tateno H, Toyota M, Saito S, Onuma Y, Ito Y, et al. (2011) Glycome diagnosis of human induced pluripotent stem cells using lectin microarray. J Biol Chem 286: 20345–20353.
32. Fujitani N, Furukawa J, Araki K, Fujioka T, Takegawa Y, et al. (2013) Total cellular glycomics allows characterizing cells and streamlining the discovery process for cellular biomarkers. Proc Natl Acad Sci U S A 110: 2105–2110.

Tissue Engineering Part A

Addition of Mesenchymal Stem Cells Enhances the Therapeutic Effects of Skeletal Myoblast Cell-Sheet Transplantation in a Rat Ischemic Cardiomyopathy Model

Yasuhiro Shudo, MD,[1] Shigeru Miyagawa, MD, PhD,[1] Hanayuki Ohkura, PhD,[1,2] Satsuki Fukushima, MD, PhD,[1] Atsuhiro Saito, PhD,[1] Motoko Shiozaki, PhD,[1] Naomasa Kawaguchi, PhD,[3] Nariaki Matsuura, MD, PhD,[3] Tatsuya Shimizu, MD, PhD,[4] Teruo Okano, PhD,[4] Akifumi Matsuyama, MD, PhD,[2] and Yoshiki Sawa, MD, PhD[1]

[1]Department of Cardiovascular Surgery, Osaka University Graduate School of Medicine, Suita, Japan.
[2]Laboratory for Somatic Stem Cell Therapy, Foundation of Biomedical Research and Innovation, Kobe, Japan.
[3]Department of Pathology, Osaka University Graduate School of Medicine, Suita, Japan.
[4]Institute of Advanced Biomedical Engineering and Science, Tokyo Women's Medical University, Tokyo, Japan.

Address correspondence to:
Yoshiki Sawa, MD, PhD
Department of Cardiovascular Surgery
Osaka University Graduate School of Medicine
Suita
Osaka 565-0871
Japan
E-mail: sawa-p@surg1.med.osaka-u.ac.jp

Received: September 2, 2012
Accepted: September 25, 2013

ABSTRACT

Introduction: Functional skeletal myoblasts (SMBs) are transplanted into the heart effectively and safely as cell sheets, which induce functional recovery in myocardial infarction (MI) patients without lethal arrhythmia. However, their therapeutic effect is limited by ischemia. Mesenchymal stem cells (MSCs) have prosurvival/proliferation and antiapoptotic effects on co-cultured cells *in vitro*. We hypothesized that adding MSCs to the SMB cell sheets might enhance SMB survival post-transplantation and improve their therapeutic effects.

Methods and Results: Cell sheets of primary SMBs of male Lewis rats (r-SMBs), primary MSCs of human female fat tissues (h-MSCs), and their co-cultures were generated using temperature-responsive dishes. The levels of candidate paracrine factors, rat hepatocyte growth factor and vascular endothelial growth factor, *in vitro* were significantly greater in the h-MSC/r-SMB co-cultures than in those containing r-SMBs only, by real-time PCR and enzyme-linked immunosorbent assay (ELISA). MI was generated by left-coronary artery occlusion in female athymic nude rats. Two weeks later, co-cultured r-SMB or h-MSC cell sheets were implanted or no treatment was performed (n=10 each). Eight weeks later, systolic and diastolic function parameters were improved in all three treatment groups compared to no treatment, with the greatest improvement in the co-cultured cell sheet transplantation group. Consistent results were found for capillary density, collagen accumulation, myocyte hypertrophy, Akt-signaling, STAT3 signaling, and survival of transplanted cells of rat origin, and were related to poly (ADP-ribose) polymerase-dependent signal transduction.

Conclusions: Adding MSCs to SMB cell sheets enhanced the sheets' angiogenesis-related paracrine mechanics and, consequently, functional recovery in a rat MI model, suggesting a possible strategy for clinical applications.

Cell Transplantation, Vol. 23, pp. 1305–1319, 2014

0963-6897/14 $90.00 + .00
DOI: http://dx.doi.org/10.3727/096368913X665602
E-ISSN 1555-3892
www.cognizantcommunication.com

Improvement of Cardiac Stem Cell Sheet Therapy for Chronic Ischemic Injury by Adding Endothelial Progenitor Cell Transplantation: Analysis of Layer-Specific Regional Cardiac Function

Sokichi Kamata,* Shigeru Miyagawa,* Satsuki Fukushima,* Satoshi Nakatani,†
Atsuhiko Kawamoto,‡ Atsuhiro Saito,* Akima Harada,* Tatsuya Shimizu,§
Takashi Daimon,¶ Teruo Okano,§ Takayuki Asahara,‡ and Yoshiki Sawa*

*Department of Cardiovascular Surgery, Osaka University Graduate School of Medicine, Suita, Japan
†Division of Functional Diagnostics, Department of Cardiovascular Medicine,
Osaka University Graduate School of Medicine, Suita, Japan
‡Division of Vascular Regeneration Therapy, Institute of Biomedical Research and Innovation, Kobe, Japan
§Institute of Advanced Biomedical Engineering and Science, Tokyo Women's Medical University, Tokyo, Japan
¶Department of Biostatistics, Hyogo College of Medicine, Nishinomiya, Hyogo, Japan

The transplantation of cardiac stem cell sheets (CSC sheets) is a promising therapeutic strategy for ischemic cardiomyopathy, although potential ischemia in the transplanted area remains a problem. Injected endothelial progenitor cells (EPCs) can reportedly induce angiogenesis in the injected area. We hypothesized that concomitant CSC sheet transplantation and EPC injection might show better therapeutic effects for chronic ischemic injury model than the transplantation of CSC sheets alone. Scaffold-free CSC sheets were generated from human c-kit-positive heart-derived cells. A porcine chronic ischemic injury model was generated by placing an ameroid constrictor around the left coronary artery for 4 weeks. The animals then underwent a sham operation, epicardial transplantation of CSC sheet over the ischemic area, intramyocardial injection of EPCs into the ischemic and peri-ischemic area, or CSC sheet transplantation plus EPC injection. The efficacy of each treatment was then assessed for 2 months. Speckle-tracking echocardiography was used to dissect the layer-specific regional systolic function by measuring the radial strain (RS). The epicardial RS in the ischemic area was similarly greater after treatment with the CSC-derived cell sheets alone (19±5%) or in combination with EPC injection (20±5%) compared with the EPC only (9±4%) or sham (7±1%) treatment. The endocardial RS in the ischemic area was greatest after the combined treatment (14±1%), followed by EPC only (12±1%), compared to the CSC only (11±1%) and sham (9±1%) treatments. Consistently, either epicardial CSC sheet implantation or intramyocardial EPC injection yielded increased capillary number and reduced cardiac fibrosis in the ischemic epicardium or endocardium, respectively. Concomitant EPC injection induced the migration of transplanted CSCs into the host myocardium, leading to further neovascularization and reduced fibrosis in the ischemic endocardium, compared to the CSC sole therapy. Transplantation of CSC sheets induced significant functional recovery of the ischemic epicardium, and concomitant EPC transplantation elicited transmural improvement in chronic ischemic injury.

Key words: Cardiac stem cells (CSCs); Endothelial progenitor cells (EPCs); Chronic ischemic injury; Strain imaging; Left ventricular remodeling

INTRODUCTION

Transplantation of somatic tissue-derived stem cells has been shown to be a feasible, safe, and potentially effective treatment for advanced cardiac failure in clinical settings (6,32). In particular, cardiac stem cells (CSCs), represented by c-kit-positive cells in the myocardium, can play a central role in healing the damaged myocardium, through their direct differentiation in situ, the recruitment of circulating stem/progenitor cells, or the paracrine release of cardioprotective factors (9,12,30). CSC transplantation is therefore considered a promising treatment for advanced cardiac failure, although the optimal method for cell delivery into the heart is still under debate (7).

The transplantation of scaffold-free cell sheets was shown to enhance the retention and survival of the transplanted cells and to minimize the risks of cell delivery-related myocardial damage that leads to arrhythmogenicity, thus showing good therapeutic potential (5,20,33). However,

Received July 26, 2012; final acceptance March 17, 2013. Online prepub date: April 3, 2013.
Address correspondence to Professor Yoshiki Sawa, Department of Cardiovascular Surgery, Osaka University Graduate School of Medicine, 2-2 Yamadaoka, Suita, Osaka 565-0871, Japan. Tel: +81-6-6879-3154; Fax: +81-6-6879-3163; E-mail: sawa-p@surg1.med.osaka-u.ac.jp

concerns remain regarding the integration of the transplanted cells into the myocardium, which would have a direct impact on regional cardiac function, and the potential for ischemia in the transplanted cell sheet, which would limit its therapeutic potential. On the other hand, endothelial progenitor cells (EPCs) have been shown to induce neoangiogenesis in the ischemic/infarcted myocardium and to activate residential CSCs to enhance healing and/or regeneration of the damaged myocardium (11,13,31). The intramyocardial injection of EPCs is thus another promising treatment for enhancing myocardial regeneration and possibly supporting the cellular function of transplanted CSCs (16).

We thus hypothesized that CSC transplantation by the cell sheet technique might induce cardiomyogenic differentiation in situ, reverse left ventricular (LV) remodeling, and improve functional recovery in ischemic injury model and that these therapeutic effects might be enhanced by the concomitant transplantation of EPCs, which could have different effects on the damaged myocardium from CSCs.

Several lines of evidence suggested that region-specific, especially layer-specific, LV function assessed by recently developing modalities may be superior to globally measured ejection fraction (EF) in predicting myocardial recovery after a wide range of medical and surgical treatment (3,14). Here we used a porcine chronic ischemic injury model to dissect the layer-specific functional effects of these two types of cell transplantation.

MATERIALS AND METHODS

All human and animal studies were carried out with the approval of the institutional ethical committee. Human samples were collected under written informed consent. The investigation conforms to the Principles of Laboratory Animal Care formulated by the National Society for Medical Research and the NIH guidelines for the care and use of laboratory animals. All experimental procedures and evaluations were carried out in a blinded manner.

Isolation and Cultivation of C-Kit-Positive Cells From Human Cardiac Tissue

Human normal right atrial tissues were obtained from a 53-year-old female patient with dilated cardiomyopathy at Osaka University Hospital. The isolation method was as published recently (6). Briefly, after dissecting fat and fibrous tissue, the sample was cut into small pieces (<1 mm^3) and suspended in 8 ml Ham's F12 medium (Wako Pure Chemical Inc., Osaka, Japan) containing 0.2% collagenase (17454; Serva Electrophoresis, Heidelberg, Germany). After digestion, cells were plated in culture dishes (353003; BD Falcon, Franklin Lakes, NJ, USA) containing Ham's F12 supplemented with 10% fetal bovine serum (FBS; SH30406.02; Hyclone, Thermo Scientific, Waltham, MA, USA), 10 ng/ml recombinant human basic fibrobrast growth factor (bFGF; 100-18B; PeproTech, Rocky Hill, NJ, USA), 0.2 mM L-glutathione (G6013; Sigma-Aldrich, St. Louis, MO, USA), and 5 mU/ml erythropoietin (E5627-10UN; Sigma Aldrich). Subsequently, cells were expanded and subjected to fluorescence-activated cell sorting (FACSAria; BD Biosciences, San Jose, CA, USA) with antibody {cluster of differentiation 117-phycoerythrin [CD117(AC126)-PE]; also known as c-kit or stem cell growth factor receptor, 130-091-735; Miltenyi Biotec, Bergisch Gladbach, Germany} to obtain c-kit-positive CSCs. The sorted c-kit-positive CSCs were cultured until the fifth passage in the above medium (30).

Preparation of CSC Sheet and Endothelial Progenitor Cells

Cultured CSCs were characterized by fluorescence-activated cell sorting (FACS) analysis, labeled by 2 μM DiI-red (Molecular Probes, Eugene, OR, USA) (33), and then incubated on 10-cm thermoresponsive dishes (Cell Seed Inc., Tokyo, Japan) at 37°C for 12 h. The DiI-red-labeled CSCs spontaneously detached from the dish surface following incubation at 20°C for 30 min, yielding a CSC sheet. Each CSC sheet was approximately 42 mm in diameter and 100 μm thick. Granulocyte colony-stimulating factor-mobilized EPCs of human origin (AllCells, MPB-017F; Emeryville, CA, USA) were labeled with 2 μM DiI-blue in vitro (Molecular Probes) (33). The following monoclonal antibodies were used: c-kit allophycocyanin (APC) [A3C6E2 (clone), 130-091-733; MiltenyiBiotec], CD105 PE (FAB10971P; R&D Systems, Minneapolis, MN, USA), CD34 fluorescein isothiocyanate (FITC) (555821, BD Biosciences), CD31 PE (FAB3567P, R&D Systems), 7-aminoactinomycin D peridinin–chlorophyll protein–cyanine 5.5 [7AAD PerCP-Cy5-5; 51-68981E (559925); BD Biosciences], immunoglobulin G1(IgG1)–FITC isotype controls (555748; BD Biosciences), IgG1–APC isotype controls (130-092-214; Miltenyi Biotec), and IgG1–PE isotype controls (IC002P; R&D Systems).

Generation of the Swine Chronic Ischemic Injury Model and Cell Transplantation

A 2.5-mm ameroid constrictor (Tokyo Instruments, Inc., Tokyo, Japan) was placed around the proximal left anterior descending artery via a left thoracotomy in female swine (Clawn miniature, 1 year old, 25 kg; Japan Farm, Inc., Kagoshima, Japan). A total of 65 swines were then cared for in a temperature-controlled individual cage with a daily intake of 5 mg/kg cyclosporin A (Novartis, East Hanover, NJ, USA) (15). Multidetector CT identified 52 pigs that developed a left ventricular ejection fraction (LVEF) between 30% and 40% at 21 days post-ameroid placement. Since eight of these pigs died prior to cell transplantation, a total of 44 pigs were randomly divided

into four treatment groups ($n=11$ in each): sham operation (sham group), CSC sheet transplantation only (CSC-only group), intramyocardial injection of EPCs (EPC-only group), and CSC sheet transplantation plus EPC injection (CSC–EPC group). After a median sternotomy under general anesthesia, three-layered CSC sheet (total 1×10^8 cells) was placed on the epicardium of the ischemic area [left anterior descending (LAD) region] and stitched in place around the edge. EPCs (total 2.5×10^6 cells) were intramyocardially injected into 12 different sites of the ischemic and peri-ischemic area. After the transplantation and/or intramyocardial injection was completed, the pericardium was closed. The pigs were taken care of for 1 day ($n=1$ each), 3 weeks ($n=4$ each), or 8 weeks ($n=6$ each), when they were sacrificed in a humane manner.

Continuous Electrocardiogram Monitoring

The electrocardiogram (ECG) was monitored during 5 days posttreatment with the Holter system (Unique Medical Co., Tokyo, Japan) for swines sacrificed at 8 weeks after cell transplantation ($n=6$ each group). The heart rate and arrhythmia events during the first 24 h were analyzed using software (Softron Co., Tokyo, Japan).

Multidetector CT and Conductance Catheterization

Global LV function was assessed by multidetector computed tomography (CT) at pretreatment and 8 weeks posttreatment ($n=6$ each) and by cardiac catheterization at 8 weeks posttreatment ($n=5$ each). After infusing 45 ml of nonionic contrast agent (Iomeron 350; Eisai Co., Tokyo, Japan) via the ear vein, 5-mm slice images of the entire heart were obtained in the craniocaudal direction using a 16-slice CT scanner (Emotion 16; Siemens, Tokyo, Japan). Every 10% of the R-R interval was reconstructed to calculate the LVEF and end-diastolic/systolic volume (EDV and ESV, respectively) using software (Lexus, Aze Inc., Tokyo, Japan).

Pressure–volume (P-V) cardiac catheterization was performed after median sternotomy by inserting a conductance catheter (Unique Medical) and a microtip catheter transducer (SPR-671; Millar Instruments, Inc., Houston, TX, USA) into the LV cavity. The P-V loop data under stable hemodynamics or inferior vena cava occlusion were analyzed with Integral 3 software (Unique Medical).

Speckle-Tracking Echocardiography and Myocardial Contrast Echocardiography

Short-axis echocardiographic images, obtained using the Artida 4D Echocardiography System (Toshiba Medical Systems Co., Tochigi, Japan) and PST-30SBT transducer, were analyzed by the speckle-tracking method using wall motion-tracking software (Toshiba Medical Systems) (2,4). End-systolic radial strain (RS) values at the mid and apical levels were averaged in a layer-specific manner to measure the endocardial and epicardial wall motion index (WMI), respectively.

Myocardial contrast echocardiography was performed using real-time contrast pulse sequencing operating on the Aplio ultrasound system (Toshiba Medical Systems) (8). Briefly, after an intravenous injection of 20 ml of ultrasound contrast agent (Sonazoid, Daiichi Sankyo Inc., Parsippany, NJ, USA), images in the apical two-chamber view were acquired to score the myocardial opacification using Volmac software (YD Ltd., Nara, Japan).

Histology

Cultured CSCs on eight-well Lab-Tec chamber slides were fixed with 4% paraformaldehyde (163-20145, Wako Pure Chemical Inc.), labeled, and examined by confocal microscopy (FV300, Olympus, Tokyo, Japan). Alexa Fluor-488 phalloidin (Molecular Probes) was used to enhance the background actin filaments. Paraffin-embedded transverse sections at the papillary muscle level were stained with Masson's trichrome (MT; Masson's Trichrome staining kit, Muto Pure Chemicals, Tokyo, Japan), and the amount of interstitial collagen at the entire LV wall was semi-quantified by MetaMorph software (Molecular Devices, Sunnyvale, CA, USA) ($n=6$, in each). In addition, the thickness of the ventricular wall was measured at two points from the LV posterior area and two points from the interventricular septum, and results were expressed as the average of the four points. Five-micrometer cryosections were subjected to either periodic acid-Schiff (PAS) staining (PAS staining kit, Muto Pure Chemicals) or immunohistolabeling. The following primary antibodies were used: rabbit anti-c-kit (1:50; Dako Co., Glostrup, Denmark), rabbit anti-von Willebrand factor (vWF; 1:500; Dako), mouse anti-Ki-67 (1:50; Dako), rabbit anti-connexin 43 (1:200; Sigma Aldrich), mouse anti-cardiac troponin I (cTn-I; 1:100; Abcam Co., Cambridge, UK), mouse anti-stromal cell-derived factor 1(SDF-1; 1:50; Abcam), rabbit anti-vascular endothelial growth factor (VEGF; 1:100; Thermo Scientific), and rabbit anti-insulin-like growth factor 1 (IGF-1; 1:100; Abcam). Capillary density was expressed as the average number of vWF-positive circular structures in five randomly selected sections, corrected for the total area of the tissue section measured. PAS-stained sections were used to determine the cell diameter of the cardiomyocytes at the remote zone. DiI-red-positive cells were traced by MetaMorph software to quantify the area of engrafted clusters of CSC sheet.

Reverse Transcription Polymerase Chain Reaction (RT-PCR)

Total RNA was extracted from the CSCs and the swine heart tissues posttreatment using an RNeasy Kit (Qiagen, Hilden, Germany), then reverse-transcribed using Omniscript Reverse Transcriptase (Qiagen) and

amplified using the Gene Amp® PCR System 9700 (Life Technologies, Tokyo, Japan). The primer pairs were as follows: human-specific kinase insert domain receptor (KDR or VEGF receptor 2) primer sequence, sense CCT CTA CTC CAG TAA ACC TGA TTG GG, antisense TGT TCC CAG CAT TTC ACA CTA TGG; human-specific chemokine C-X-C motif receptor 4 [CXCR4 or stromal-derived factor 1 (SDF-1) receptor] primer sequence, sense ACG TCA GTG AGG CAG ATG, antisense GAT GAC TGT GGT CTT GAG; human glyceraldehyde-3-phosphate dehydrogenase (GAPDH) primer sequence, sense AAT GGG CAG CCG TTA GGA AA, antisense GCG CCC AAT ACG ACC AAA TC; swine-specific SDF-1 primer sequence, sense CCGAACTGTGCCCTTCAGAT, antisense ATAA ACATCCCGCCGTCCTC; swine-specific CXCR-4 primer sequence, sense GCGCAAAGCTCTCAAAACCA, antisense CAGTGGAAAAAGGCAAGGGC; swine-specific VEGF primer sequence, sense GAC GTC TAC CAG CGC AGC TAC T, antisense TTT GAT CCG CAT AAT CTG CAT G; swine-specific IGF-1 primer sequence, sense ACA TCC TCT TCG CAT CTC TTC TAC TT, antisense CCA GCT CAG CCC CAC AGA; swine GAPDH primer sequence, sense CTG CAC CAC CAA CTG CTT AGC, antisense GCC ATG CCA GTG AGC TTC C. The transcript level of GAPDH was used as an endogenous reference. The products from the cultured CSCs were stained with ethidium bromide (Bio-Rad Laboratories, Hercules, CA, USA), separated by electrophoresis (Mupid submarine electrophoresis system, Advance Co. Ltd., Tokyo, Japan) on an agarose gel (Agarose S, Nippon Gene Co., Ltd., Tokyo, Japan), and quantified.

Fluorescence In Situ Hybridization (FISH)

Paraffin-embedded sections were predenatured, dehydrated, and then labeled with deoxyribonucleic acid probes, a Cy3-conjugated probe for human-specific genome, Cy5-conjugated probe for swine-specific genome (Chromosome Science Laboratory, Hokkaido, Japan), and mouse anti-cTn-I or rabbit anti-vWF. The sections were visualized with secondary antibodies conjugated to Alexa fluorochromes. Nuclei were labeled with 4,6-diamino-2-phenylindole (DAPI; Molecular Probes).

Statistical Analysis

Continuous data are summarized as medians with ranges (minimums to maximums) or means ± SEM (standard error of mean) and are plotted in figures with raw values or barplots of the means with symmetric SEM bars, as appropriate. Distributions of the continuous data were checked for normality with the Shapiro–Wilk test and for equality of between-group variances with the Levene test. Normally distributed data were compared between four groups using the analysis of variance (ANOVA), followed by the Tukey multiple comparison for equal variances, or Welch's ANOVA, followed by the Games–Howell multiple comparison for unequal variances. Nonnormally distributed data were compared using the Kruskal–Wallis test, followed by the Steel–Dwass multiple comparison. Normally and nonnormally distributed data before and after treatment were compared using the paired t test and the Wilcoxon signed rank-sum test, respectively. All p values are two-sided, and values of $p<0.05$ were considered to indicate statistical significance. All analyses were performed with the SPSS 11.0J for Windows (SPSS, Chicago, IL, USA) and the R program (http://www.r-project.org/) (10).

RESULTS

Human Atrium-Derived C-Kit-Positive Cells Showed CSC Characteristics In Vitro

The isolated right atrium-derived cells were characterized in vitro by FACS, immunohistolabeling, and RT-PCR analyses. The proportion of c-kit-positive cells at the second passage was 99 ± 4% (Fig. 1A and B). However, as the cells expanded, they lost the primitive phenotype, and more than half of them had the potential to differentiate to the endothelial rather than the cardiomyocyte or smooth muscle cell lineage. The proportion of c-kit-positive cells at the fifth passage was 20 ± 10%, while 34%, 71%, and 99% of them expressed CD34, CD31, and CD105, respectively (Fig. 1C). Immunohistochemistry revealed that approximately 5% of the cells expressed cTn-I in the cytoplasm (Fig. 1D). In addition, RT-PCR clearly revealed the expression of CXCR4 and KDR in the cells (Fig. 1E).

After incubating the cells on temperature-responsive dishes at 37°C for 12 h, CSC sheets were generated by lowering the temperature. Each cell sheet was approximately 42 mm in diameter, and the gap junction protein connexin 43 was expressed between the cells (Fig. 1F). Most of the cells expressed the proliferation marker Ki-67 in their nucleus (Fig. 1G).

Successful Cell Transplantation With Minimal Arrhythmogenicity

A total of 44 pigs underwent treatment, which was performed without any procedure-related mortalities ($n=11$ each). Fatal arrhythmias, such as ventricular tachycardia and fibrillation, or composite ventricular arrhythmias (grades 3–5 in Lown's classification) were not detected in any group during the first 24 h posttreatment, as assessed by Holter ECG monitoring ($n=6$ each) (Table 1). There were no significant differences in the heart rate or number of unifocal premature ventricular/atrial contractions among the groups.

Global Functional Recovery After CSC Sheet Transplantation Was Enhanced by EPC Injection

Multidetector CT measured LVESV, LVEDV, and LVEF, and cardiac catheterization measured the systolic